Intermetallic phase transformations during homogenisation of 6xxx Al alloys

A literature review

Ir. N.C.W. Kuijpers[1]

February, 2000

Supervisors:
Dr. I. Todd[1]
Dr. W.H. Kool[2]
Prof. Dr. Ir. S. van der Zwaag[1,2]

[1]Netherlands Institute for Metal Research, Delft
[2]Laboratory for Materials Science, Delft University of Technology

P.004.004

Contents

1 Introduction

The composition given in Table 1.1 is typical of that for 6063 Al alloy, which is the most used 6xxx series extrusion alloy. The table shows that the Fe content is quite high (0.35 wt%). This unintentionally high Fe content is the case in most of the alloys comprising the 6xxx aluminium series, and is the result of both the recycling of aluminium and the production process. During casting almost all Fe remains in the liquid (because Fe has a very low solubility in solid) but at the end of the casting process iron rich intermetallics are formed on the boundary of the grain. The process and mechanism of the solidification process will be reviewed in chapter 3.

Table 1.1 Alloy content of 6063 Al [Shep99].

Mg	Fe	Si	Cr, Zn, Ti	Mn
0.45-0.9 wt%	0.35 wt%	0.20-0.6 wt%	0.10 wt%	0.10 wt%

Industrial homogenisation is performed at approximately 585 °C for a few hours to dissolve precipitates and make a more refined structure of grains and intermetallics inside the billet. This results in a higher ductility and also better extrusion properties of the billet. This review focuses on b to a AlFeSi intermetallics transformation during the homogenisation process. In the course of this transformation the AlFeSi phases change shape, composition, crystal structure, size and distribution, in a way which is favorable for the extrusion properties of the material. Experimental details of this transformation process are given in chapter 4.

Chapter 5 introduces some physical models to describe the transformation of b- to a- intermetallics, where dissolution kinetics, multiple phases and change in morphology are taken into account. To model the phase transformation quantitatively, numerical computer models are necessary. A review of different types of numerical approaches to diffusion and dissolution problems are covered in a complementary report [Til00].

2. Ternary AlFeSi phases

2.1 The Al-Fe-Si phase diagram and crystal structures of a *- and* b *- precipitates*

Figure 2.1 shows the positions of the phase fields for the various different types of stable intermetallics which can be formed in Al-Fe-Si alloys [Mond76]. These phases may also form in other Al-alloys systems, where Fe and Si are present as constituent phases.

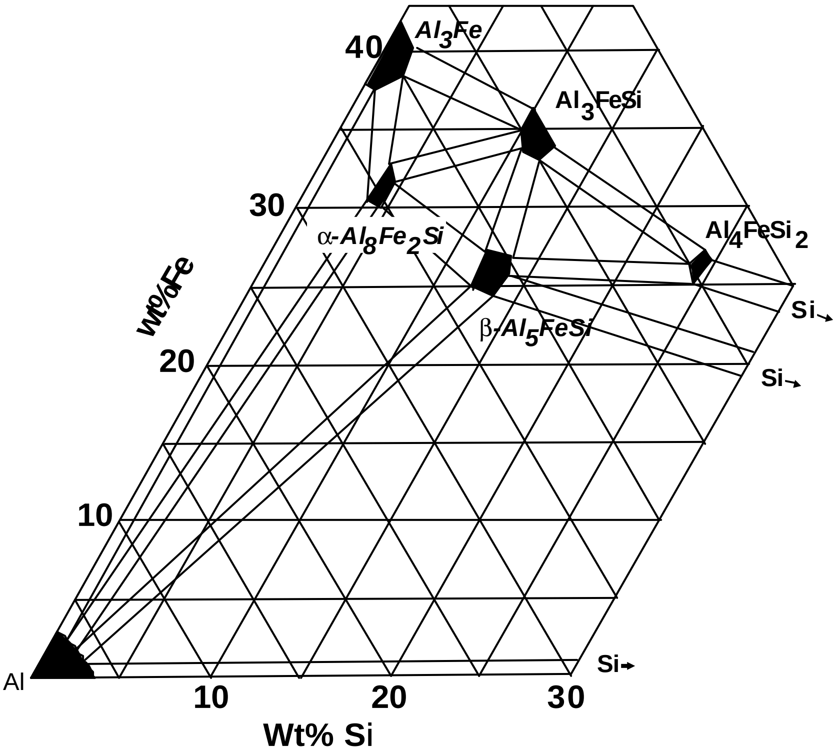

Figure 2.1 The aluminium corner of the solid state phase diagram [Mond76].

For 6xxx alloys containing sufficient amount of Fe and Si the equilibrium structure for Fe and Si containing intermetallics is the hexagonal *a*¢-Al$_8$FeSi phase [Tani99, Dons84], which is also shown in Figure 2.1. It is found that minor additions of elements like V, Cr, Mn, Cu, Mo and W stabilize a cubic a_c-Al$_{12}$Fe$_3$Si phase. In some literature the general term "*a* "-phase is used, without giving the structure of this phase. In this report this α-phase represents the set of α_c and α¢ phases, which both have almost similar stoichiometries.

During casting of 6xxx primarily metastable cubic a_c and/or monoclinic *b*-Al$_5$FeSi phases are formed. The *b*-phase is also shown in the stable solid state phase diagram of Figure 2.1, but in 6xxx Al alloys this *b*-phase is unstable because the corresponding phase field of the 6xxx alloy belongs to the *a*¢-Al$_8$Fe$_2$Si (or α_c phase in the presence of certain elements). Probably this metastable *b*-phase is formed because of non-equilibrium solidification conditions, where the liquid becomes enriched in Si, due to partitioning of Si in the interdendritic liquid.

Table 2.1 presents the most frequently observed phases in 6xxx series alloys, which are the monoclinic *b*-types, cubic a_c, and hexagonal *a*¢. Table 2.2 presents the more infrequently observerved AlFeSi-intermetallics in 6xxx alloys or AlFeSi-intermetallics which are found in other alloy compositions.

Table 2.1. The structural variance of the *a* and *b* AlFeSi phases: most commonly observed Phases in 6xxx series.

Phase	Bravais lattice	Lattice parameters	References
b	Monoclinic	a=6.12 Å b=6.12 Å c=41.5 Å b=91 deg	[Skjer87]
a_c (a_1)	Cubic: bcc or primitive cubic.	a=12.56 Å (Im3) a=12.52 Å (Pm3)	[West82] [Mond76] [Grig89] [Turm87]
a¢ (a_2)	Hexagonal	a=b=12.3 Å c=26.2 Å	[Dons85] [Grig89]

Table 2.2. The structural variance of the *a* and *b* AlFeSi phases: Infrequently observed phases in 6xxx series; Intermediate phases during casting of 6xxx Al Alloys; observed in other alloys than 6xxx aluminium Alloys.

Phase	Bravais lattice	Lattice parameters	References
β′, β*	Monoclinic	a = 8.9 Å b = 4.9 Å c = 41.6 Å b = 92 deg	[West82] [Skjer87]
α_R	Rhombohedral superlattice $R\bar{3}$	a_{sup} = 3.076 c_{sup} = 3.623	[Liu88]
α″(q_1)	c-Centred orthorhombic	a = 12.7 Å b = 26.2 Å c = 12.7 Å	[West82] [Liu86]
α_T	c-Centred monoclinic	a = 27.95 Å b = 30.62 Å c = 20.73 Å b= 97.74 Deg	[Dons84] [Liu86]
q_2	Monoclinic	a = 12.50 Å b = 12.30 Å c = 19.70 Å b = 111 deg	[Liu86]
α_v	Monoclinic	a = 8.90 Å b = 6.35 Å c = 6.32 Å	[Dons84]

2.2 Frequently observed AlFeSi intermetallics in 6xxx series

Monoclinic *b*-phase

The *b*-AlFeSi has a monoclinic crystal structure and a plate like morphology, and is an important phase in wrought aluminium alloys [Alle98]. The probable stoichiometry of this phase is Al_5FeSi. Figure 2.2 shows a TEM image and diffraction pattern of the *b*-AlFeSi. Mulazimoglu *et al.* [Mula96] found that the *b*-AlFeSi is highly facetted and contains multiple (001) growth twins parallel to the growth direction. Further, Mulazimoglu *et al.* suggested that the reported value of c=41.5 Å is due to the existence of a superstructure in the β phase and that the unit cell is based on c=20.8 Å rather than on 41.5 Å. More details concerning the formation of the *b*-phase during casting will be given in chapters 3 and 4.

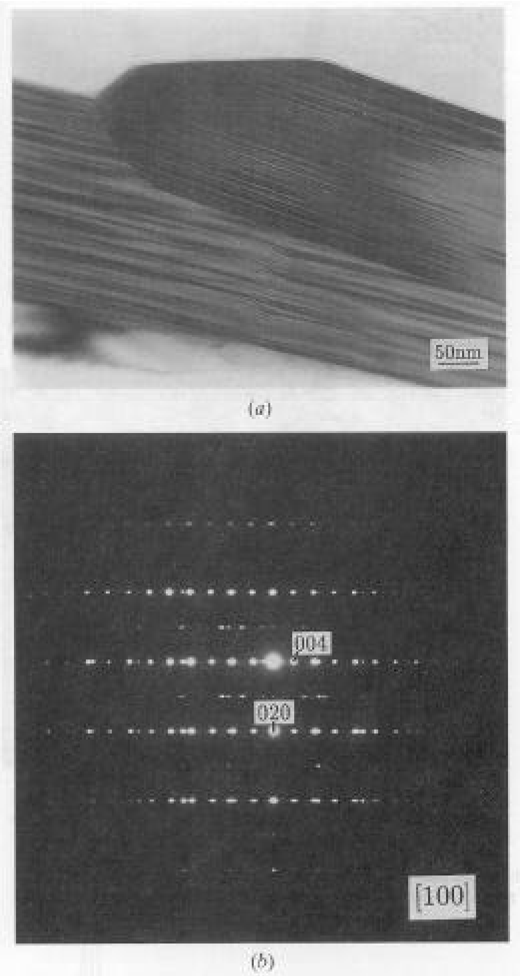

Figure 2.2. *(a) TEM image of a b- particle (b) electron diffraction pattern [mula96].*

Cubic α_c phase

In 6xxx series containing high iron content of ~0.5 wt% or cooled at very high cooling rates (50 K/s) the cubic a-phase (a_c) is formed upon solidification, where the morphology of this phase is more spheroidised in comparison to the plate-like β phase. For pure Al-Fe-Si alloys small additions of V, Cr, Mn, Cu, Mo and W stabilize a_c and it seems to be the thermodynamically stable phase as it is observed even after long homogenisation times [Alle98]. Unlike the monoclinic *b*-phase, the a_c-phase exhibits no faceting or twinning and has a rough or diffusive interface with the matrix [Mula96], as can be seen in Figure *2.3*. Donnadieu *et al.* [Donn94] found that a_c has an $Al_{12}Fe_3Si$ stoichiometry, which is isostructural to the $Al_{12}Mn_3Si$ phase.

Westingen *et al.* [West82] observed cubic a_c in DC-cast 1050 alloy in the more rapidly cooled outer zone of the billet. Weak $h + k + l =$ *odd integer* spots were observed in the diffraction patterns, indicating that the structure may not been body centered but primitive cubic.

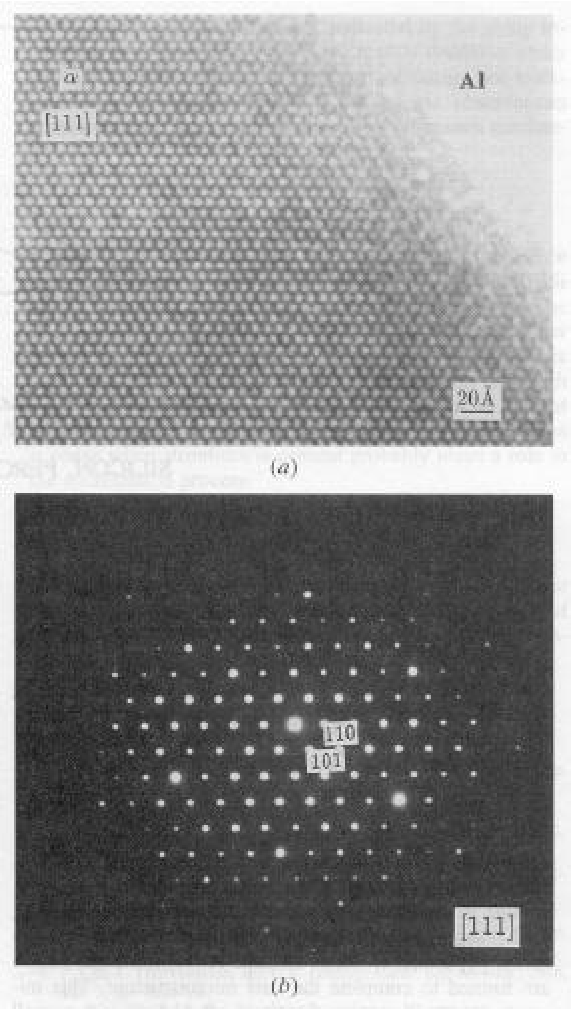

Figure 2.3. *(a) HREM image of interface between a-AlFeSi and the aluminium matrix. (b) Electron diffraction pattern of a-AlFeSi. [Mula96].*

Hexagonal *a¢* phase

The hexagonal *a¢* (also called a_2) is probably the equilibrium state of FeSi containing intermetallics in high purity AlFeSi alloys [Dons84]. Additions of Ti, Ni, Zn, and Mg promote formation of intermetallics with this hexagonal structure and therefore gives *a¢* as the equilibrium state. For 6063 series probably *a¢* is the equilibrium state [Tani99, Dons84]. This is derived from the observation that during homogenisation of 6xxx alloys the *a¢* phase is formed from the *b* particles [Tani99, Zaja94]. Chapter 4 and 5 will give more details of this transformation process. Figure 2.4 gives a picture of an *a¢* particle with corresponding diffraction pattern.

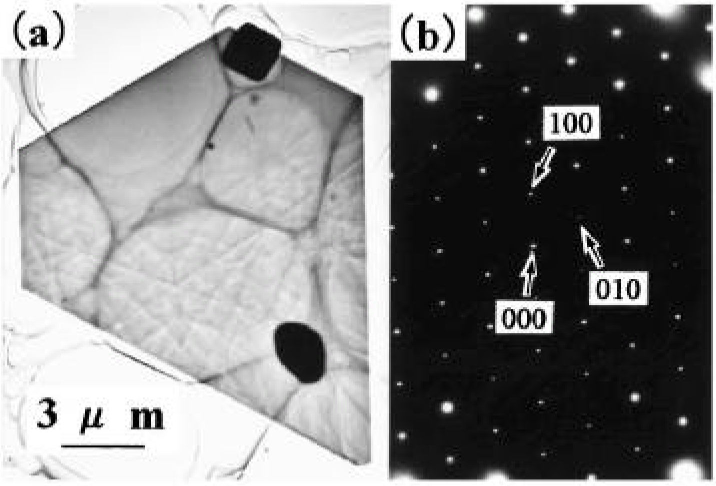

Figure 2.4. [Tani99] (a) TEM picture of a′ with corresponding (b) selected area diffraction pattern (Beam //[001] of the a′-AlFeSi).

2.3 Infrequently observed metastable AlFeSi phases

Metastable *b¢* Al-Fe-Si phase

Westengen *et al.* [West82] occasionally found *b¢* particles in DC-cast material with a composition corresponding to AA1050. The monoclinic *b¢* shows twin boundaries, as in the *b*-phase. Also the magnitude of the c-axis of 41.6 Å corresponds to that of the c-axis of the *b*-AlFeSi. It can be discussed that this high *c*-value is the result of twinning (as also discussed for β particles). The other lattice parameters (*a*=8.9 Å and *b*=0.49 Å) deviate from the corresponding values for *b*-particles. EDS data gives that the Fe/Si ratio is higher than two, while the *b*-AlFeSi phase have a Fe/Si ratio of one, therefore Westenger concluded that this phase may be a low Si modification of β.

Metastable α_R-Al-Fe-Si phase

Liu *et al.* [Liu88] found a rhombohedral superstructure with a space group $R\bar{3}$ and lattice parameter a_{sup}=30.6 Å , c_{sup}=32.63 Å in bcc *a*-AlFeSi intermetallics. The superstructure is formed by a long-range ordering of iron vacancies in the structure. The superstructures have been determined using many methods, i.e. SAED, convergent beam electron diffraction (CBED), energy dispersive x-ray spectroscopy (EDX), and high resolution imaging [Liu88].

Metastable *a¢¢* or q_1-Al-Fe-Si phase

Westengen [West82] observed *a¢¢*-particles in alloys with AA1050 like compositions. The structure of this particle is closely related to a_c-particles: two axes are identical and the third is about a factor three higher. Westengen also found that *a¢¢* has a lower Si content than cubic a_c. Liu *et al.* [Liu86] also observed α″ (but he named it q_1) in DC-cast Al-0.28 wt% Fe-0.13 wt% Si at a cooling rate of ~10 Ks^{-1}. Detailed convergent beam electron diffraction analyses by Liu *et al.* on α″ revealed a c-face centred orthorhombic crystal structure.

Metastable α_T-AlFeSi phase

The a_T phase was observed by Dons [Dons84] and is related to the cubic a phase (a_c). Conform Skjerpe [Skjer87] the diffraction patterns of a_T may be described as weak superstructure reflections imposed on the basic bcc structure of the a_c-AlFeSi. The composition is close to that of bcc a_c -AlFeSi and the two phases sometimes display identical diffraction patterns. The phases may therefore easily be confused and therefore most cases, it is better to make not a distinction between these two phases.

Metastable q_2-AlFeSi phase

Liu *et al.* [Liu86] found that the q_2 phase was formed by the transformation of α¢¢ (q_1) phase after annealing for 24 h at 600 °C of an chill cast Al-0.28 wt% Fe-0.13 wt% Si billet. The composition of this phase corresponds to an $Al_{20}Fe_4Si$ phase. Liu *et al.* found that the crystal lattice of this phase had a monoclinic unit cell, and convergent electron diffraction showed that q_2-AlFeSi has a Pm space group.

Metastable α_v–AlFeSi phase

Dons [Dons84] observed a_v-type of particles in DC-cast commercial purity Al-0.2 wt% Fe-0.2 wt% Si alloys, and stated that this phase is a monoclinic structural variant of a-AlFeSi. Furthermore Dons suggested that this phase is related to the Al_9Fe_2 phase, where the a-axis was 2.6 % shorter and the c-axis 3.6 % shorter than in Al_9Fe_2. The Al_9Fe_2 phase is also metastable and infrequently reported in literature. The compositions are also different in comparison to Al_9Fe_2: the Al_9Fe_2 –phase contains less than 2 wt% Si, while the Si-content inside the a_v particle ranges from 4.5 to 10.5 wt%.

3. AlFeSi intermetallics formed during the casting process

During casting, intermetallics are formed between the arms of the solidifying aluminium dendrites. Fe has a very low solubility in the solid aluminium (~ 0.05 wt% at equilibrium), and therefore the Fe remains in the liquid aluminium until the last moments of solidification, and solidifies in the form of a second phase intermetallic. As a result, almost all Fe in the alloy is present in different kinds of metastable second phase intermetallics between the aluminium grains [Sjer87].

3.1 The formation of a_c- and b-phases in 6xxx Al alloys castings

Langsrud [Lang90] found that the starting Fe/Si [wt%/wt%] composition ratio of the alloy is an important parameter which determines whether cubic a_c- or monoclinic b-AlFeSi particles are formed in the cast. When the Fe/Si ratio is higher than approximately 1 during solidification the liquid phase field touches the a phase field and a particles are formed. When the Fe/Si is lower than approximately 1, during the solidification the liquid touches the b phase field and b particles are formed. The same Fe/Si composition effect was as found by Tanihata *et al.* [Tani99], as presented in Figure 3.1.

The measurements of Tanihata *et al.* were obtained in cast 6063 series of aluminium with composition of 0.1 to 0.5 wt% Fe-0.4 wt% Si – 0.5 wt% Mg – 0.001 wt% Mn. At industrial cooling rates of 5 K/s and industrial Fe content of 0.2 wt% (with corresponds to Fe/Si=0.43) only monoclinic b-AlFeSi particles were formed. These results confirm the fact that b-AlFeSi is the main phase found in industrial as-cast 6063 alloys. At an industrial cooling rate of 5 K/s and 0.5 wt% Fe (which corresponds to Fe/Si=1.2) a_c-particles are formed instead of b-particles within a wide range of cooling rates of 0.01 K/s to 50 K/s.

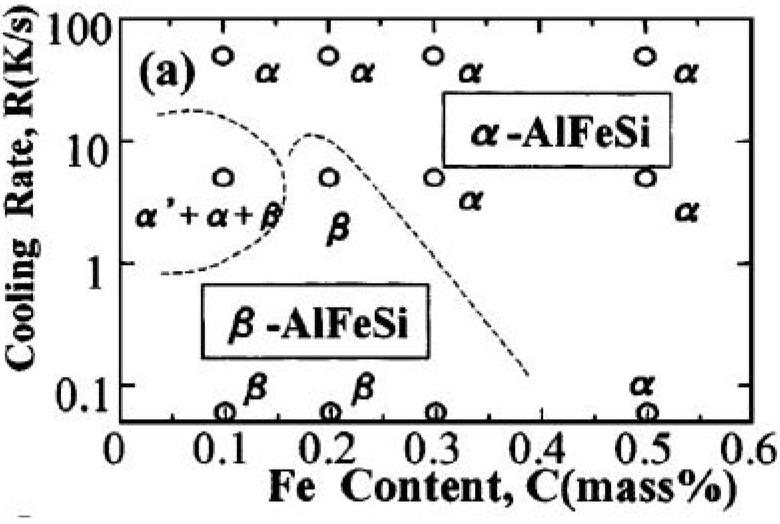

Figure 3.1 The range of relative amounts of AlFeSi intermetallics in the ingot as-cast material [Tani99]. (“a” is the a_c phase.)

Langsrud stated that the metastable phase fields of a and b particles change as a function of the cooling rate. Therefore more silicon rich particles (like b) will be formed when the cooling rate is higher. This contradicts to the results of Tanihata *et al.* as presented by Figure *3.1*, where a particles are formed at higher cooling rates, which contain less Si than b-particles.

The morphologies of a_c-AlFeSi and b-AlFeSi particles (with the same dimensions) are very different [Grig89]. According to TEM and SEM observations, the a_c-AlFeSi (in AA6063 with a high iron content of 0.5wt% Fe and an industrial cooling rate of ~5 K/s) consists of strongly curved crystals which in some place grow together into plates with irregular, curved surfaces. These curved plates follow the dendrite boundary at higher solidification rates. In a flat polished surface this spatial phase morphology appears in the form of “Chinese script” [Grig89, Turm87].

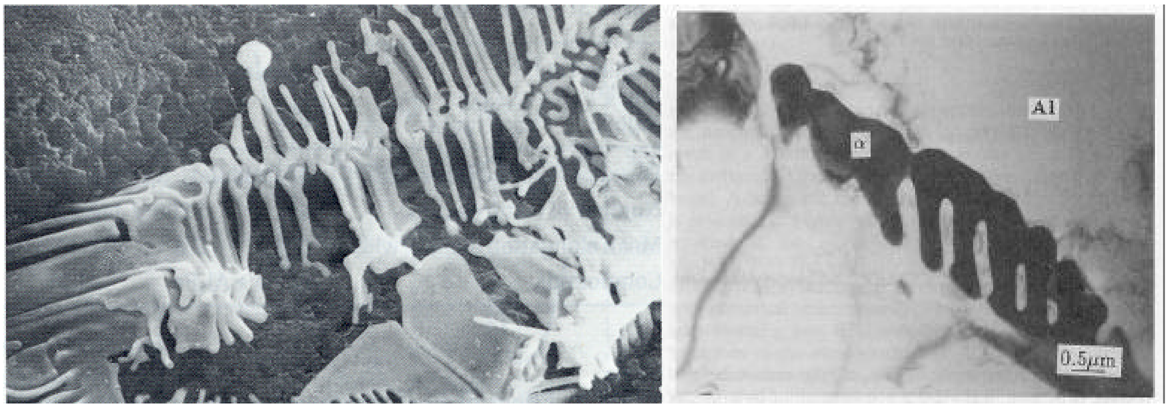

Figure 3.2.(a) Deepetches a_c particle in 99.95% pure 0.5% Fe and 0.2%Si (cooling rate between 2 K/s and 11 K/s)[Grig89]. (b) TEM picture, showing chinese script [Mula96].

The b-AlFeSi crystallizes as moderately curved planes (Figure 3.2), which are observed as needles in a micrograph [Grig89].

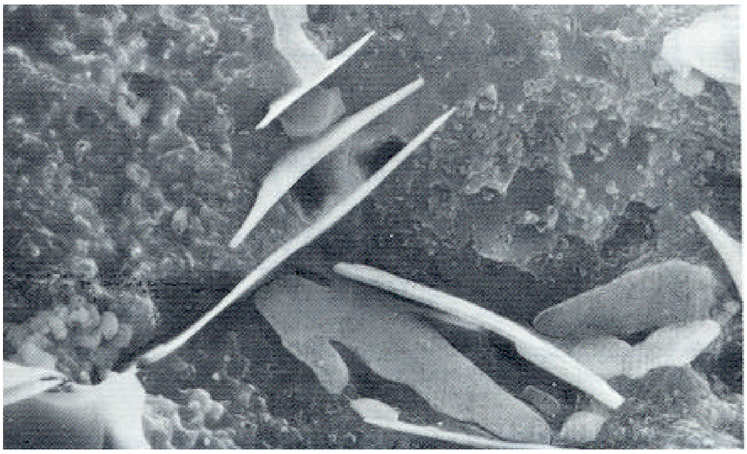

Figure 3.3 *Deep etch of b particles in 1% Si and 0.5% Fe aluminium alloy [Grig96].*

Some investigations report observing both the a_c and the b phase in one as-cast material [Birol98]. The b-particles are formed at the boundary of the dendrites, and the a_c phase is found as the described Chinese-script like morphology at the triple points of the grains, as shown in Figure 3.4. It can be surmised that a_c is formed by a local higher iron content at the triple points.

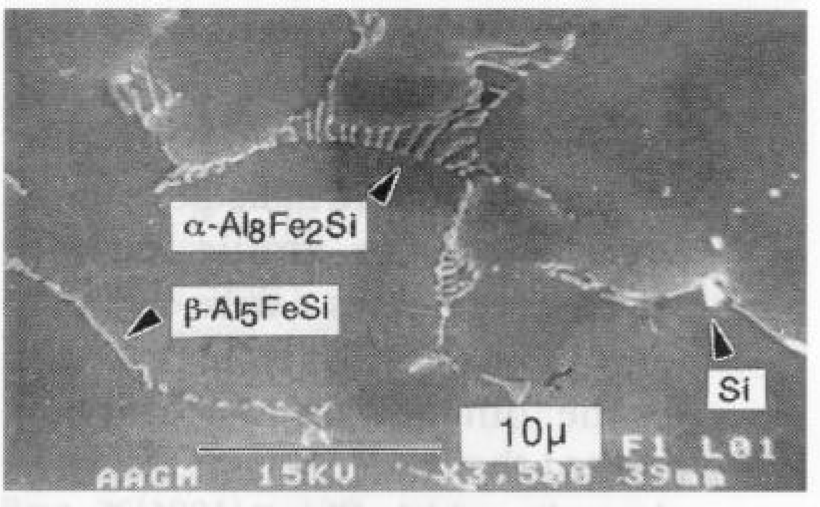

Picture 3.4 A SEM image which illustrates a_C-AlFeSi in the form of chinese script and plate like b-AlFeSi- [Birol98]. Both the a and the b phases are present in the alloys. Also Si phases are present in the alloy. The concentration of this alloy is equal to: 0.707 wt% Fe - 0.770 wt% Si - 0.038 wt% Cu - 0.006 wt% Mn.

3.2 The mechanism of forming *a* or *b* particles during casting

Langsrud [Lang90] discussed that *a* and *b* particles are formed directly from the liquid, and the metastable phase fields corresponding to the *a* and *b* phases changes as the cooling rate changes. He worked with equilbrium diagrams, where hexagonal α´ is the equilibrium phase. However, in cast structures α_c is found, as was presented in the previous section.

Other reported mechanisms are that *b* particles are formed as a result of peritectic reactions from *a* to *b* particles. Langsrud wrote that this is very unlikely because the solidification is much too fast in comparison to solid-reactions and the resulting microstructure does not show any typical features of peritectic reactions, like peritectic rings. Peritectic rings were also not found by Mulazimoglu *et al.* [Mula96], however they found some unreacted *a*-AlFeSi attached to *b*-AlFeSi, which seems to support to the occurrence of peritectic reactions. Different types of reported peritectic reactions are reviewed in this section.

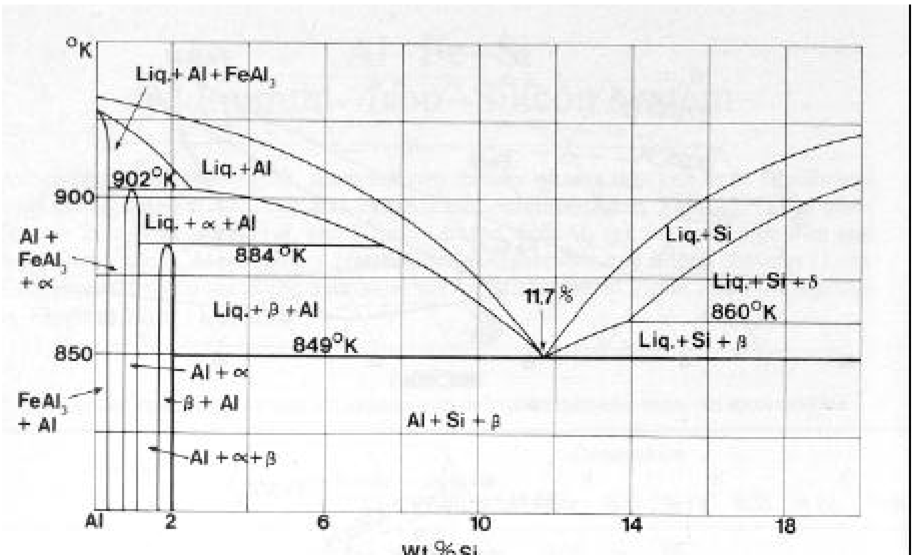

Figure 3.5 A section of the aluminum-iron-silicon diagram at 0.7% Fe [Mond76].

To give formula's for the phase transformation which may occur during solidification, we can employ the assumption that there is no solid-diffusion and the only reactions are between the liquid and growing solid. Figure 3.5 gives a section of the Al-Fe-Si diagram at 0.7 wt% Fe. Under non-equilibrium solidification conditions, the liquid becomes enriched in Si and Fe and therefore the route of non-equilibrium is difficult to obtain. However, from the figure it is possible to derive that the following reactions may occur during casting:

$T \approx 933$ K Liquid → Al dendrite (3.1)
$T \approx 928$ K Al-Liquid + Al-dendrite → Al + Al_3Fe (3.2)
$T \approx 903$ K Liquid + Al_3Fe → Al + a (3.3)
$T \approx 885$ K Liquid + a → Al + b (3.4)
$T \approx 869$ K Liquid → Al + Si + b (3.5)

The reaction temperatures given [Mond76] are dependent on the local concentrations of the aluminium matrix, which can be very different in alloys containing other solute elements. Therefore the temperatures given here are only an indication.

Reaction (3.1) is the solidification of aluminium while no new phases are formed. The liquid becomes enriched with Fe and Si, and at a certain temperature the reaction (3.2) may begin. With further cooling of the liquid, the Al_3Fe reacts to solid aluminium and the a-phase (3.3). At lower temperatures the a-phase reacts with the aluminium and forms solidified aluminum and b-particles. The remaining liquid forms a ternary eutectic at (3.5).

Mulazimoglu *et al.* [Mula96] investigated the 6201 Al alloy with composition 0.6 wt% Mg-0.6 wt% Si – 0.3 wt% Fe- 0.003 wt% Mn. This alloy has a low Fe/Si ratio of 0.5 and is formed at an industrial cooling rate of 10 K/s, and thus b particles are formed during casting, corresponding to the predictions of Langsrud. Mulazimoglu *et al.* suggested that due to a supercooling phenomena almost only b particles are formed between the dendrites. They stated that although Al_3Fe is an equilibrium phase at that temperature it is difficult to nucleate, therefore step (3.2) and (3.3) almost do not occur. And most a phases are formed directly from the liquid like the formula:

Liquid → Al-dendrite + a. (3.6)

However, these a-particles are expected to be very small. Mulazimoglu *et al.* stated that the a phase can only grow for a short period of time in a short temperature range (between 618 to 615 ^{o}C) before the peritectic temperature is reached (3.4). Competitive nucleation of b phases will start (as described in section 3.4), whereafter the small a-plates are easily decomposed to the b-phase. Tanihata *et.al.* [Tani99] discussed the possibility that at casting the solid state reactions have to be taken into account. He found that at very high cooling rates of 50 K/s only cubic a particles were found, which corresponds to the solid state equilibrium at high temperatures, while at lower cooling rates monoclinic b-particles were found (see Figure *3.1*) which is the equilibrium phase at lower temperatures. This is not predicted by the theory of Mulazinoglo: his theory would predict b-particles at high cooling rates. Therefore Tanihata suggested that during cooling down with lower cooling rate the a-particles were transformed to the β particles with a peritectoid (solid-solid) reaction:

Al + a → b. (3.7)

However, when a critical cooling-rate is exceeded a-phase cannot transform into the b-phase and a is left over.

3.3 Addition of strontium to form a_c phase during casting

Some articles deal with the addition of strontium to AA6063 material [Mula96]. Therefore a brief overview of this subject is presented in this section. Addition of about 30 ppm strontium promotes the formation of cubic a_c-phase during casting, giving a coarser morphology to the intermetallics than otherwise reached with the b-phase. It has been postulated that the a_c-phase should give these alloys better extrusion properties, but there has been little investigation of this aspect yet. It has been suggested that strontium adsorbs to the growing interface of the a_c-phase. This prevents Si dissolution into the a_c particle, which is a necessary step for the formation of b-types of particles. A picture reported to show this effect is given in Figure 3.6.

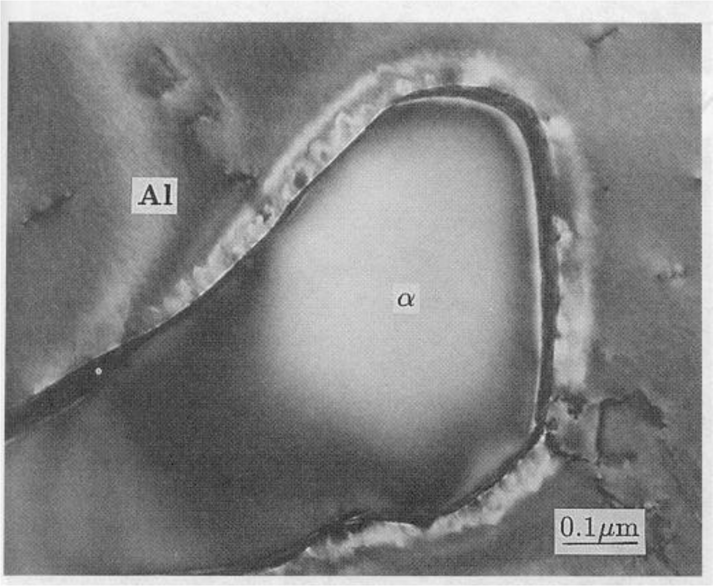

Figure 3.6 Silicon-rich layer surrounding a_c-AlFeSi phase in the presence of strontium [Mula96].

3.4 Competitive growth and nucleation

Figure 3.1 showed that a-phase is formed at higher cooling rates (50 K/s) and that the b is formed at lower cooling rates. A reason for this effect can be the shifting of a and b phase field as described in section 3.1; however, competitive growth and/or competitive nucleation can also be a reason for the formation of a at high cooling rates.

During competive growth one phase (say A) suppress the formation of another (say B), because the growth temperature of one phase is higher than the other:

$$T_{grow\,A} > T_{grow\,B}$$

To illustrate the effect of competitive growth an example of the results of Backerüd [Back68] will be discussed. Backerüd studied the eutectic growth temperature T_{growth} for the eutectics (1) Al/Fe_4Al_{13} and (2) Al/$FeAl_6$ in Al- 0.5 to 4.0 wt% Fe alloys. Figure 3.7 shows the results of the experiments, from which it can be derived that below a critical cooling rate of $(dT/dt)_{critical}$=3.3 Ks^{-1} it yields that $T_{growth\,1} > T_{growth\,2}$ and therefore at those cooling rates the eutectic Al/Fe_4Al_{13} will suppress Al/$FeAl_6$. At cooling rates higher than 3.3 Ks^{-1} the eutectics Al/$FeAl_6$ will grow faster than the eutectics Al/Fe_4Al_{13} and the order of predominance is reversed.

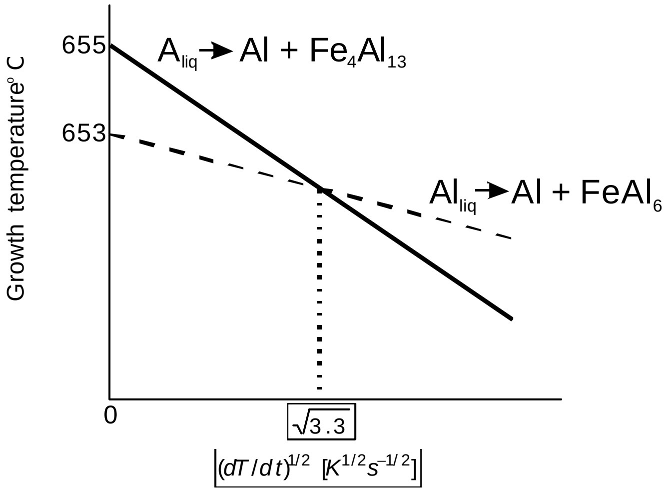

Figure 3.7 The variation of eutectic growth temperature for Al/Fe_4Al_{13} *and Al/*$FeAl_6$ *eutectics [Alle98].*

Similar to competitive growth the phase *B* can be kinetically displaced by another phase *A* if the nucleation temperatures are such that

$$T_{nuclate\ A} > T_{nucleate\ B}\ ,$$

where it is assumed that both phases can grow under the given solidification conditions.

4. Phase transformations of b- to a-intermetallics during homogenisation

4.1 Introduction

The AlFeSi-interdendritic intermetallics influence significantly the mechanical properties of 6xxx series aluminium-alloys. To give the alloy better deformation or extrusion characteristics, the alloy is homogenised where the plate like monoclinic b intermetallics transform to the more favorable rounded a intermetallics. It is found that for pure Al-Fe-Si systems the final transformation product is the hexagonal α' phase, however if minor alloy additions of other elements, e.g. Mn, stabilize the cubic a_c phase. It is found that aluminium with a higher volume fraction α particles has a better hot workability and less pickup during extrusion than aluminium with only b phases [Lang86, Clod86]. The reason for these better properties will be discussed in section 4.6.

The morpology change of the AlFeSi phase in 6063 series of alloy (containing 0.05% Mn) during the phase transformation of b to a is shown in the two micrographs in Figure 4.1: The plate like b particle transformed after a homogenisation at 565 °C of 6 hours to a chain of smaller and more rounded a particles. The figure was obtained with optical microscopy, where the sample was etched with 0.5% HF to increase the grey level difference between black b and grey a particles [Zajac].

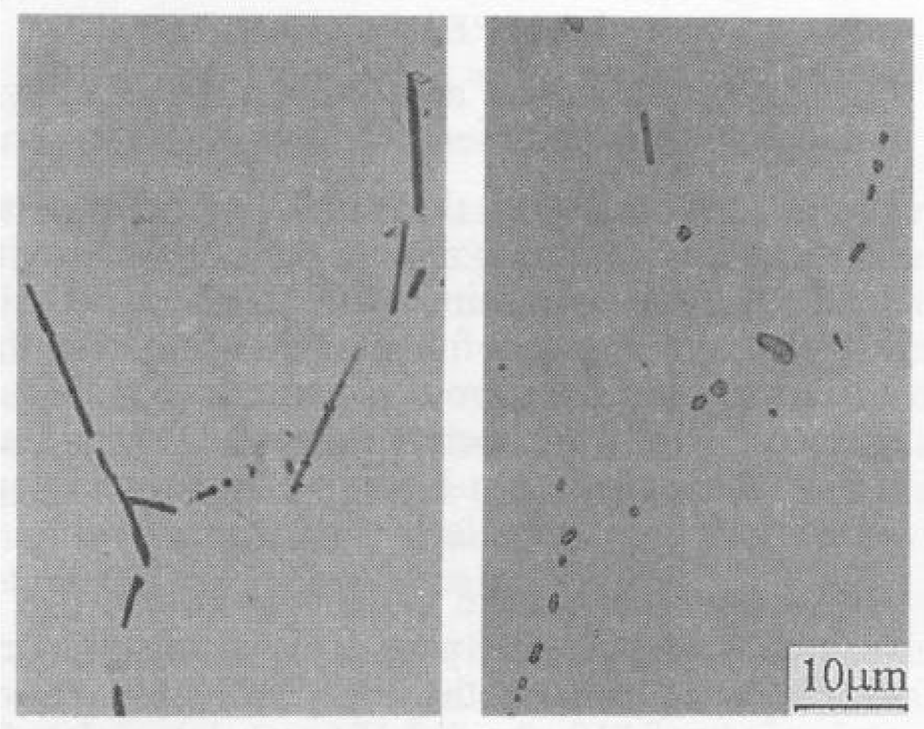

Figure 4.1 The b to a transformation in 6063 series of aluminium. The grain size is ~156 mm (a) as-cast (b) homogenised 565^{o}C for 6 hours. (optical, etched with 0.5% HF) [Zaja96].

Little has been documented about the kinetics and mechanism of the b to a transformation. In this respect, Zajec *et al.* [Zajec94, Zaja96] is the main source of literature. They looked at the effect of additions of manganese to the alloy and the effect of the grain size (sections 4.4 and 4.5) on the transformation in 6063 and 6005 Al alloys. Further, the mechanical properties were investigated and correlated to the *coverage ratio*, which is the percentage of grain boundary length covered by particles (section 4.5). Birol [Biro98] looked at the transformation of particles at the surface of a strip-cast Al-0.8 wt% Fe –0.6 wt% Si alloy, and at the influence of cold-rolling before the heat-treatment. Tanihata *et al.* [Tani99] reported on the transformation after homogenisation for 8 hours and 667 hours with different Fe concentrations and cooling rates of 6063 alloys. Finally, Onurlu *et al.* [Onur94] wrote about the effect of heat treatment in 6063 where they investigated the transformation as a function of time and temperature by x-ray examination of extracted phases. All these results will be reviewed in this chapter.

4.2 Experimental results on b to a transformation

Birol [Birol98] found in Al-0.8wt% Fe-0.6wt% Si-0.009 wt% Mn alloys (undeformed) that in the intermediate transformation time of 8 hours both the a_c and the a' is formed, and after a longer homogenisation time (72 hours) only the stable a' is found. The measurements were performed by x-ray diffraction (XRD) on pulverized surface layers. The results are presented in Table 4.1, where the main phase is underlined, and the rare phases are in brackets.

TABLE 4.1 INTERMETALLICS PRESENT AT DIFFERENT HOMOGENISATION CONDITIONS [Birol98].

heat treatment	Observed particles
540 –8 hours	$\underline{b}$, a_c, (a')
560 –8 hours	a_c, b, a'
580 –8 hours	a_c, b, a'
600 –8 hours	$\underline{a_c}$, a'
600 –72 hours	$\underline{a'}$

Birol found that the transformation rate was somewhat accelerated in samples that have received a cold-rolling pass before the heat treatment. It is possible that the introduction of defects increases the rate of diffusion and contributes to the establishment of the equilibrium state. Furthermore mechanical break up will accelerate the tranformation ratio because of larger surface area.

Onurlu *et al.* [Onur94] measured the b to a transformation in 6063 alloys (0.24 wt% Fe-0.28 wt% Si- 0.014 wt% Mn - 0.54 wt% Mg) as a function of time and temperature, which results are presented in Table 4.2. Particles were extracted and measured by XRD, and companion TEM measurements and electron diffraction studies were carried out on 20 extracted particles of each specimen. The only observed a- particle was the bcc a_c type, which is probably caused by stabilisation of the a_c phase by manganese. No Mg_2Si-precipitates, and few Si-precipitates are found in the as-cast structure. [Onur94].

Onurlu *et al.* also found little AlFeSiMg intermetallics by SEM and energy dispersive x-ray analyses (EDAX) in the as-cast structure. However, it was observed that the Mg in the intermetallics dissolved after a homogenisation of 1 hour. By x-ray and XRD no AlFeSiMg particles were observed in the as-cast structure and therefore Ornula concluded that those phases are present only in trivial amounts.

TABLE 4.2 INTERMETALLICS PRESENT IN HOMOGENISED 6063 ALLOYS [Onur94].

homogenisation time (hours)	Temperature (^{o}C)				
	550	560	570	580	590
1	$b+a_c$	$b+a_c$	$b+a_c$	a_c	a_c
2	$b+a_c$	$b+a_c$	$b+a_c$	a_c	a_c
4	$b+a_c$	$b+a_c$	a_c	a_c	a_c
8	$b+a_c$	$b+a_c$	a_c	a_c	a_c

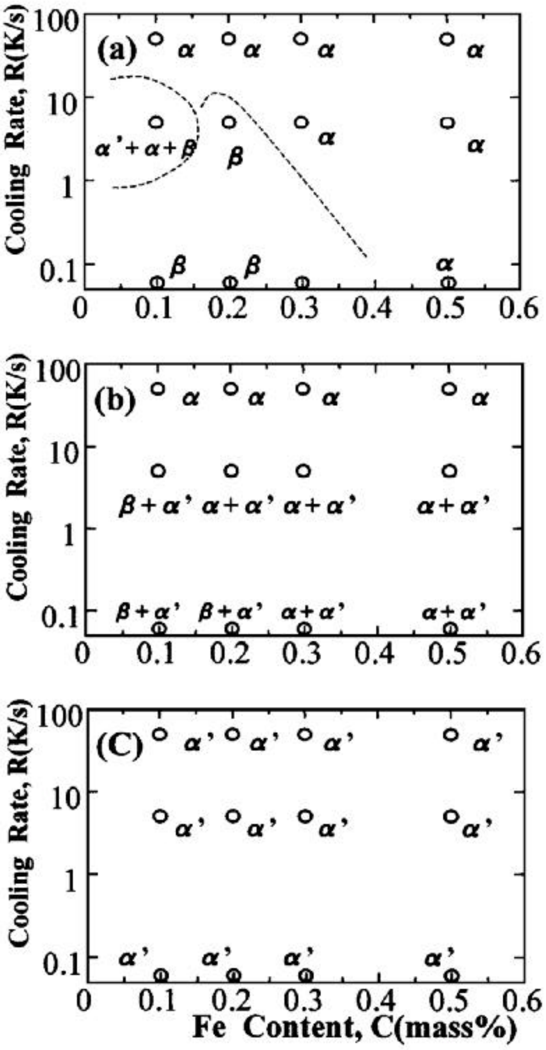

Figure 4.2. Al-Fe-Si intermetallic compounds in the ingots during homogenisation [Tani99]. The "a" in the picture is defined as the cubic a_c. (a) as cast, this graph was also shown in Figure 3.1 (b) homogenised at 858 K for 15 hours , and (c) for 667 hours.

Tanihata *et al.* [Tani99] looked at the transformation of 6063 alloys with composition of 0.1 to 0.5 wt% Fe -0.4 wt% Si- 0.5 wt% Mg and 0.001 wt% Mn where the cooling rate and iron content of different casting samples were varied. After a very long homogenisation time of 667 hours he found that for all samples the a' is the main phase, which can be seen in Figure 4.2c. Like Birol, Tanihata also found that in the intermediate homogenisation times (15 hours) the *b* phase is transformed in both the a_c and the a', as can be observed in Figure 4.2a and 4.2b for a cooling rate of 5 K/s and 0.2 wt% Fe. From the figure it can also seen that the a_c intermetallics in as cast structures (i.e at a high iron content of 0.5 wt%) transform to the more stable hexagonal a' particles after long homogenisation times.

4.3 The kinetics and mechanism of the b to a transformation

Figure 4.3 shows the growing of new *a* particles on a *b* plate, as observed by Zajec *et al.* in 6005 alloys with a composition of 0.77 wt% Si- 0.19 wt% Fe- 0.53 wt% Mg - 0.041 wt% Mn. *a* particles are probably nucleated on the boundary of *b* phases. Zajec et al. proposed that the *b* strings are gradually replaced by a uniform dispersion of cubic and/or hexagonal *a*-AlFeSi particles. The islands of *a* then thicken and spheroidize at the expense of the remaining *b*-phase.

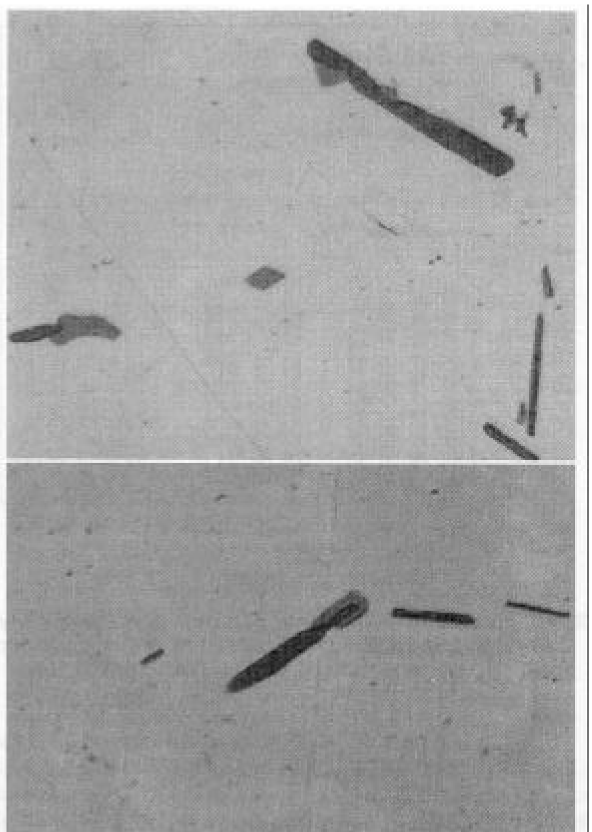

Figure 4.3 Partial transformation of b particles (black) to a particles (light grey) after homogenisation at 565 °C for 2 hours. New a-paritlces are nucleated and grown on the b- particles.(optical, etched with 0.5% HF, x 1600). In 6005 series of alloy with 0.53 Mg, 0.77 Si 0.19 Fe and 0.041 Mn (wt%).

Both Zajec *et al.* and Birol [Biro98] found that the dispersive *a* particles become coarser if the homogenisation process is longer than approximately 10 hours. The thickness of the *a* particles increases due to the coarsening mechanism, which may have a negative effect on the ductility, because dislocations only flow around particles smaller than a critical size, as described in section 4.6. Zajec *et* *al.* found that in an 6063 alloy (with 0.082 Mn) homogenised for 6 hours, 10 hours and 20 hours there are 2600, 1900 and 1500 *a*-particles/mm^2 present respectively. The decrease of the number of particles is caused by coarsening: fewer and bigger particles are formed.

Zajec, also looked at the shape factors of the particles. He found that the mean shape factor changes as a function of time, which is a result of the morphology change from platelike particles to the more rounded α particles. Zajac defined the shape factor as:

$$pd^{2}_{max}/4A \tag{4.1}$$

Where d_{max} is the maximum diameter of a particle, and A is the surface area of a particle. Therefore the shape factor can be seen as a measure of ellipticity: A spherical particle has a shape factor of 1 while a more plate like particle has a higher shape factor. Because there is a morpology change from platelike to rounded particles, Zajec *et al.* found that the mean shape factor lowers as a function of homogenisation time. For example. for 6063 alloys he found that the shape factor changes from 4.2 at 1 hours to 3.5 at 2 hours homogenisation time.

Presumably, during the *b* to *a* transformation Si diffuses in the Al-matrix to form the desired *a* particle [Birol98] according to:

$$2b\text{-}Al_5FeSi \rightarrow \alpha\text{-}Al_8Fe_2Si + [Si]_{Al} + 2Al, \tag{4.2}$$

where $[Si]_{Al}$ indicates the Si concentration which is dissolved inside the Al matrix. Birol [Birol98] analyzed the matrix after homogenisation and concluded that whilst the matrix did indeed reveal relatively higher amounts of silicon with respect to the as-cast state, and this could not be due to dissolution of Si or Mg_2Si precipitates. This silicon must therefore have come from the *b* to *a* phase-transformation, as given by reaction *4.2*.

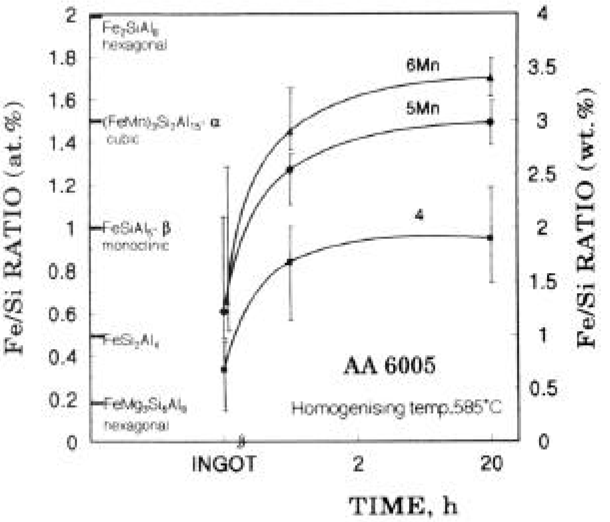

Figure 4.4 The change of Fe/Si ratio in the intermetallic phase as a function of homogenisation time of different 6005 Al alloys. The composition is: 0.2 Fe- 0.8 Si- 0.5 Mg (wt%) where the Mn concentration are <0.010, 0.041 and 0.082 wt%, as labeled in the figure as "4", "5Mn" and "6Mn" respectively.

Because Si dissolves out of the intermetallic, the Fe/Si ratio on the intermetallics changes as a function of homogenisation time, which was also obtained by Zajec *et al.* Figure 4.4 gives the Fe/Si change as a function of homogenisation time for different 6005 alloys. It can be seen that the Fe/Si ratio increases during homogenisation time, where it must be noted that the high Mn alloy concentration can influence the type of phase which is formed e.g the quaternary cubic a_c-$Al_{15}(FeMn)_3Si$ [Donn94], instead of the ternary hexagonal α´-Al_8Fe_2Si. This aspect was not discussed by Zajec.

Birol measured the Fe/Si ratio of 6063 alloys by EDS and he concluded that the *b* phase have a Fe/Si ratio of 1±0.25. For *a* particles he found an Fe/Si ratio ranging between 1.42 an 1.92. After a long homogenisation time of 72 hours at 600 °C the Fe/Si ratio of α-particles is even higher than 1.92.

4.4 Dependence transformation rate of grainsize

Zajac changed the grain size by addition of the grain refiner TiB_2 and found in the as-cast condition coarse grain structures (400 µm, 750 µm) with additional small and more rounded α-AlFeSi phase particles inside the grains. Well developed dendrites in coarse grain structures decreased the tendency for precipitation of large β particles on the grain boundaries. Therefore, the amount of α-AlFeSi particles increased with an increase in grain size.

Figure 4.5 shows the number of *a*-particles after 2 hours homogenisation as a function of the homogenisation temperature. It must be noted that it clearly can be seen that the transformation rate is highly temperature dependent. It can be seen that bigger grains (e.g 750 µm) have more α particles, however, this is caused by the fact that there are already more *a* particles in the as-cast structure. If the grain size is small enough (e.g 47 µm) the fraction *a* particles is again higher than at some bigger grain sizes (110 µm and 156 µm), as a result of higher transformation rate of the intermetallics associated with those small grains. It is probable that, when the grain size is small enough, Si can diffuse faster outside the thin *b* particles, and therefore transforms quicker to *a*-AlFeSi. Zajec did not discuss the effect of the grain refiner (TiB_2) itself on the diffusion and transformation kinetics, and assumed that they only affected the grain size.

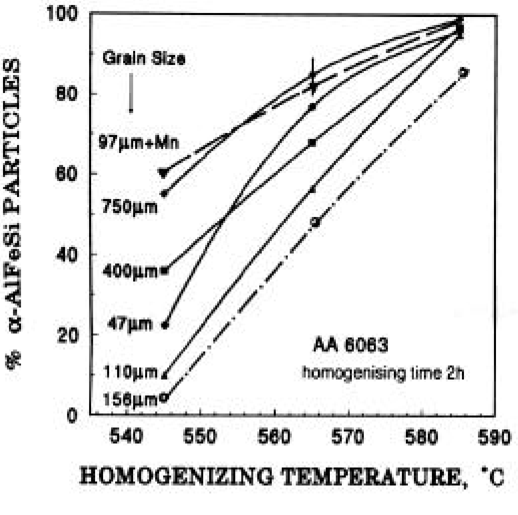

Figure 4.5 The percentage of a particles as a function of the homogenisation temperature.

4.5 Addition of manganese to accelerate the b to a transformation

The *b* to *a* transformation is significantly accelerated by additions of small amounts of manganese (e.g. 0.04 wt%) [Lamb79, Zaja94], which is a very beneficial effect for the extrusion industry. Conform Lamb [Lamb79], the introduction of manganese into the alloy gives a shift of the solid state *a*-AlFeSi phase field in the direction of lower Fe/Si ratios. In practice this means that the tranformation of the non-equilibrium *b* phase to the equilibrium *a* phase during homogenisation is accelerated.

An illustration of the effect of Mn additions to the transformation rate in 6005 Al alloy is shown in Figure 4.6, where the alloy content is presented in Table 4.3. The figure shows that at a low manganese content (<0.01 wt% Mn) and 20 hours homogenising less than 10% of the intermetallics were transformed to *a*. However, for high Mn content (0.082 wt% Mn) and the same homogenisation time, the transformed fraction is improved by approximately 100%. The figure also shows that the number of α particles decrease after a certain homogenisation time (i.e after 6 hours at 0.082 wt% Mn), which is a result of particle coarsening, as discussed in section 4.3.

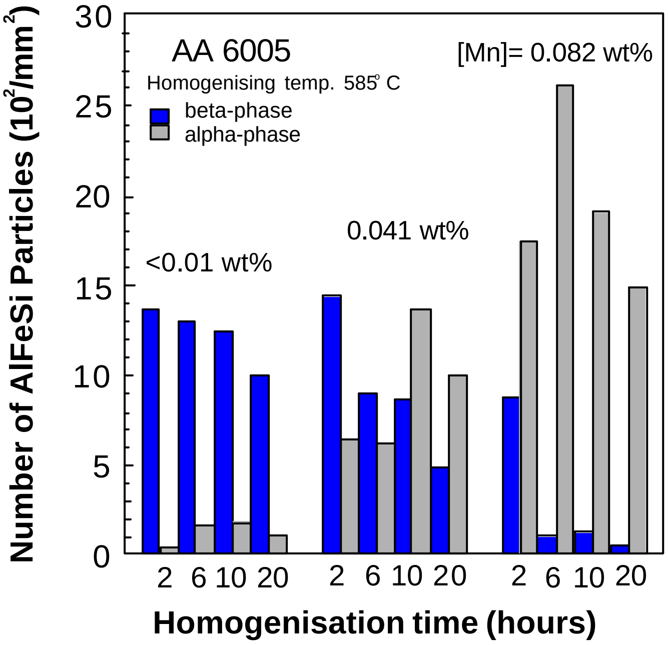

Figure 4.6 The transformation of b- to a-AlFeSi particles in systems with different Mn alloy contents [Zaja94].

TABLE 4.3 ALLOY CONTENTS OF AA6005 SAMPLES.

Mn	Mg	Si	Fe
<0.010	0.52	0.82	0.18
0.041	0.53	0.77	0.19
0.082	0.53	0.80	0.20

Donnadieu *et al.* [Donn94] identified coarse intermetallics with an cubic a_c-$Al_{12}(Fe_x,Mn_{1-x})_3Si$ stochiometry where the iron and manganese are interchangeable to each other. (if x=1 this phase becomes the cubic a_c-$Al_{12}Fe_3Si$ phase). It can be discussed that when Mn is added to 6xxx Al alloys this cubic a_c-$Al_{12}(Fe_x,Mn_{1-x})_3Si$ phase is nucleated instead of the hexagonal a'-Al_8Fe_2Si phase, and that this cubic phase with additions of Mn exhibits a higher nucleation rate and/or a faster growth rate than the hexagonal phases. This could be an alternative explanation for the more rapid *b* to *a* transformation rate observed in the presence of manganese additions, however, there is no further literature found which support this hypothesis. It is possible that Zajec *et al.* did not take the difference between a_c and a' particles into account because in his report the particles where identified by the optical grey-scale, and it is plausible that the hexagonal a' phase and cubic a_c phase exhibits the same grey intensity in reflected light optical microscopy.

4.6 Ductility as a function of intermetallic coverage ratio of the grain boundary

It has been proposed [Zaje98] that if the particles are spheroidised and smaller, the dislocations may loop around the particles, thereby increase the ductility, and the material is easier to extrude. The plate like particles blockade the dislocations at the boundary, and therefore the ductility is low if there are much plate like particles. Zajec suggested an empirical equation for the critical particle size (d_c), below which no climbing of dislocations occurs:

$$d_c = \left(\frac{KD}{T\dot{e}} \right)^{1/3}, \tag{4.2}$$

where K is a constant, D is the diffusivity, T is the temperature, and $\dot{e}$ is the strain rate. Equation 4.2 shows that at higher deformation temperatures or deformation rates the size of the particles must be smaller to prevent blockading of dislocation motion.

Zajac *et al*. found that the ductility limit of 6063 series correlated to the "*coverage ratio*", where the coverage ratio is defined as the percentage of grain boundary length covered by particles with a higher size than the critical particle size d_c. Figure 4.7 shows that the ductility limit (expressed in the temperature corresponding to 90% reduction of area) clearly correlates to the coverage ratio defined as $S_{p>6\ \mu m}$, where $d_c = 6$ µm. When the grainsize gets small, also the coverage ratio gets smaller. Therefore, it can be discussed whether the grain size or the "*coverage ratio*" is the main reason for the ductility change as observed by Zajec *et al.*

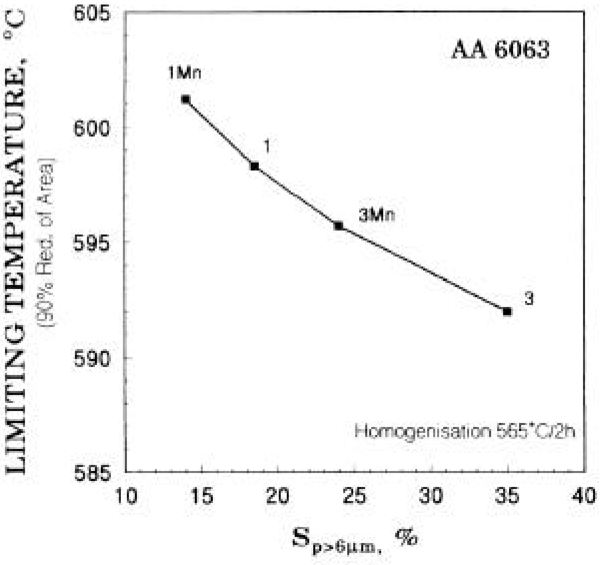

Figure 4.7 The limiting temperature as a function of the coverage ratio ($S_{p>6\ m\ m}$). 1Mn, 1, 3Mn, 3 are samples identifications from the paper [Zaj98].

5. Models of *b*- to *a*- phase transformation during homogenisation

The experimental results reviewed in the previous chapter will be supported by more physical background. The main mechanism of transformation of *b*- to *a*- intermetallics during homogenisation has not yet been determined. The *b*-intermetallic is metastable when during homogenisation a phase transformation occurs. This indicates that the *b* phase is outside its own phase field equilibrium, and the new phase which is formed corresponds to the actual phase field. The phase transformation can occur by a peritectoid reaction of the *b*-intermetallics and the aluminium matrix to give the *a*-intermetallic. Intermetallics will coarsen and spheroidise as a result of instabilities caused by chemical potential differences of the boundary. These instabilities may be the reason for the observed morpology changes that occur during the transformation.

5.1 Dissolution of a precipitate

This section deals with dissolution of a precipitate during homogenisation, where no phase transformation is taken into account. This will give a general understanding of diffusion and interface conditions, important for peritectoid phase transformations, which will be dealt with in the next section.

Dissolution kinetics are also important because they can be the reason for instabilities, and therefore can explain the morphology change obtained during the *b*- to *a*-transformation (see section 5.1.4). Another reason for dealing with dissolution is that it is possible that during homogenisation *b*-AlFeSi partially dissolves in the Al matrix before or during the phase transformation, as is shown in Figure 5.1b. A *b*-particle will dissolve according to the reaction:

$$b\text{ - Al}_5\text{ FeSi} \rightarrow 5\text{Al} + [\text{Fe}]_{\text{Al}} + [\text{Si}]_{\text{Al}}. \tag{5.1}$$

On the other hand it can also grow with the reverse formula:

$$5\text{Al} + [\text{Fe}]_{\text{Al}} + [\text{Si}]_{\text{Al}} \rightarrow b\text{ - Al}_5\text{FeSi}, \tag{5.2}$$

where in both equations diffusion inside the intermetallic is neglected, because the compositions of those elements are assumed to be stoichiometric. In the extreme situation it may be envisaged that the whole precipitate dissolves in the matrix as schematically shown in Figure 5.1c. It can be discussed that the spot with high Fe and Si concentration is a source for new *a* type particles. However, Fe has a very low solubility in Al (~0.05 wt%), so it is highly unlikely that the *b* particles dissolve completely.

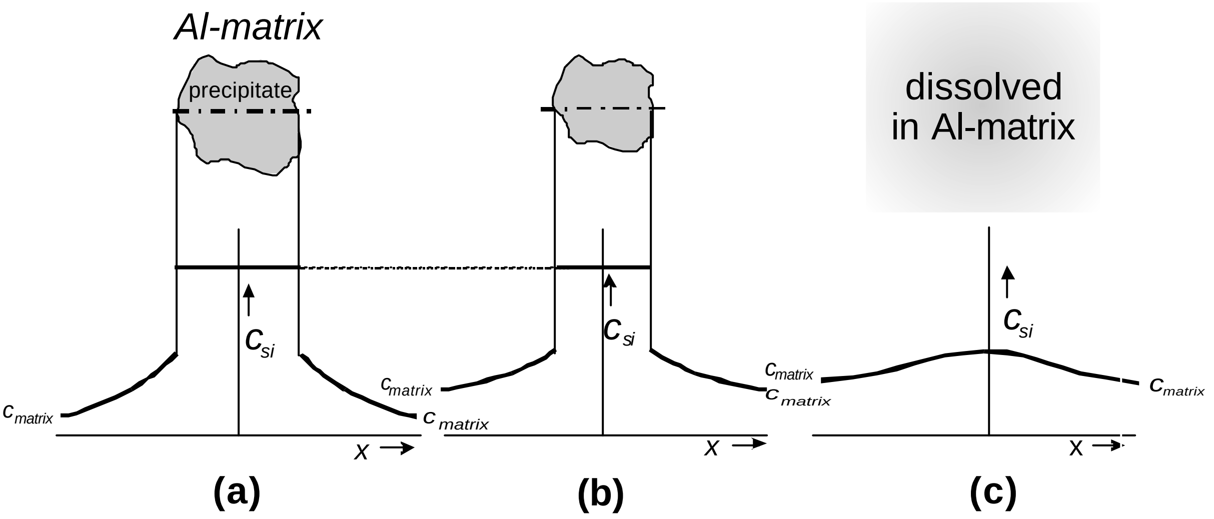

Figure 5.1 Schematical diagram of the dissolution of an intermetallic in the Al-matrix with its Si concentration profiles. (a) as-cast starting condition (b) partial dissolved particle, the mean concentration in the matrix increases (c) in the extreme situation the intermetallic is completely dissolved.

5.1.1 Diffusion inside the aluminum matrix

Diffusion inside the aluminium matrix, of common elements like Fe, Si, Mn and Mg occurs mainly by the vacancy mechanism [Port91]. Aluminium has almost no anisotropy in diffusion, so the diffusion is non-directional.

The driving force of diffusion is the chemical potential difference (*m*). The concentration of the matrix adjusts to lower chemical potential, and the concentration profile is in equilibrium if the chemical potentials at all places are equal. However, the chemical potential is a property which is difficult to measure, and therefore most diffusion processes are expressed in concentrations (*c* in wt%). Assuming that the diffusional flow of atoms of one chemical species is independent of the concentration of the other elements, the rate of diffusion of each element, relative to the Al-lattice becomes:

$$\mathrm{J}_{\mathrm{Fe}} = D_{Fe} \nabla c_{Fe} \ , \tag{5.3}$$

$$\mathrm{J}_{\mathrm{Si}} = D_{Si} \nabla c_{Si} \ , \tag{5.4}$$

$$\mathrm{J}_{\mathrm{Al}} = D_{Al} \nabla c_{Al} \ , \tag{5.5}$$

where *J* is the diffusion flux (wt%/m^2) and *D* is the intrinsic diffusion coeficient. Equation (5.1) gives the self diffusion of aluminium inside its matrix. The intrinsic diffusion coefficients are given by an Arrhenius relation of the form:

$$D_p = D_{0,p} \exp\left(-\frac{Q_{dif,p}}{RT} \right), \tag{5.6}$$

where $D_{o,p}$ is a pre-exponential factor and $Q_{diff,p}$ is the activation energy of diffusion, and p= Fe,Si, or Al. Table 5.1 gives an overview of the pre-exponential factors and activation energies of the main alloying elements in aluminium and the self diffusion coefficients of Al in the Al-matrix.

TABLE 5.1 SOME DIFFUSION COEFFICIENTS OF ELEMENTS IN 6XXX ALUMINIUM SERIES.

	Temperature range	Reference	D_0 (m^2s^{-1})	Q (kJ/mol)	D (m^2/s^{-1}) 540 °C	D (m^2/s^{-1}) 590 °C
Al	(Self diffusion)					
		Alexander *et al.*[Alex70]	$0.11\cdot10^{-4}$	29	$1.51\cdot10^{-7}$	$1.93\cdot10^{-7}$
		Porter and Easterling [Port91]	$0.170\cdot10^{-3}$	142	$1.28\cdot10^{-13}$	$4.32\cdot10^{-13}$
	753 K–873 K	Fujikawa [Fuji77]	5.07	143	$3.29\cdot10^{-9}$	$1.12\cdot10^{-8}$
Fe	793 K-922 K	Beke *et al.* [Beke87]	$5.3\cdot10^{-3}$	183.4	$8.73\cdot10^{-15}$	$4.21\cdot10^{-14}$
	823 K–906 K	Alexander *et al.*[Alex70]	$1.35\cdot10^{-2}$	192.6	$5.70\cdot10^{-15}$	$2.97\cdot10^{-14}$
	792 K–931 K	Hood [Hood70]	91	258.7	$2.18\cdot10^{-15}$	$2.00\cdot10^{-14}$
Si	618 K–904 K	Bergner *et al.* [Berg73]	$0.35\cdot10^{-4}$	123.9	$3.83\cdot10^{-13}$	$1.11\cdot10^{-12}$
	753 K-893 K	Fujikawa. [Fuji78]	$2.02\cdot10^{-4}$	136	$3.69\cdot10^{-13}$	$1.19\cdot10^{-12}$
Mg	667 K-928 K	Rothman *et al.* [Roth74]	$1.24\cdot10^{-4}$	130.4	$5.19\cdot10^{-13}$	$1.59\cdot10^{-12}$
	773 K-853 K	Fujikawa. [Fuji77]	$1.06\cdot10^{-4}$	133	$3.02\cdot10^{-13}$	$9.45\cdot10^{-13}$
Mn	773-923 K	Bergner *et al.* [Berg73]	$1275\cdot10^{-4}$	229	$2.47\cdot10^{-16}$	$1.76\cdot10^{-15}$

To compare the investigated coefficients with each other, in Figure 5.2 the different diffusion coeficients of Mg, Si and Fe are plotted against temperature. These coefficients are calculated by the Arrhenius relation of Equation (5.6) and with the coefficients of Table 5.1. It can be seen that the diffusion coefficients of the same element deviate between different references. This deviation is caused by difference in technique of measurement, difference in temperature range, or difference in type of alloy which is used for the experiments (e.g pure Al or alloyed Al).

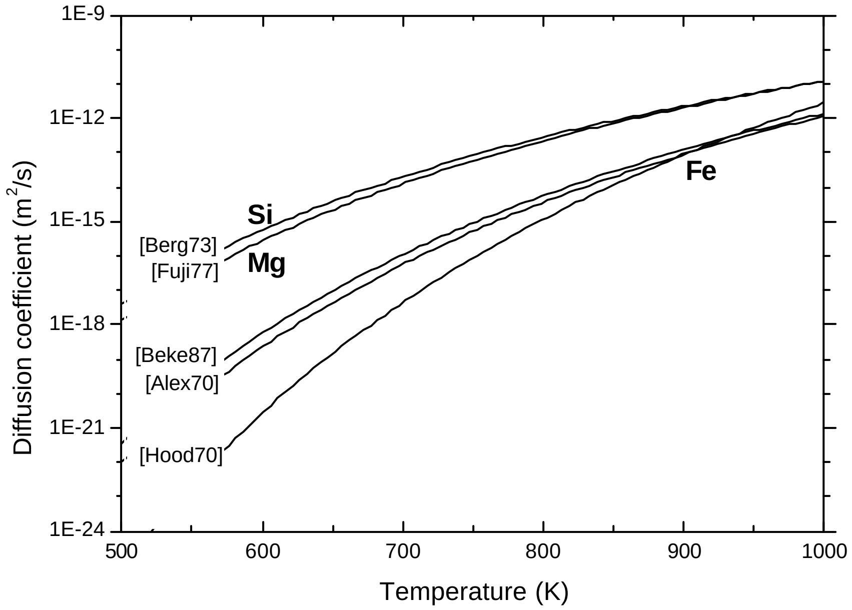

Figure 5.2 Overview of different diffusion coefficients of Mg, Si and Fe in aluminium as a function of the temperature.

5.1.2 The equilibrium concentration on the boundary

The concentration profile at the boundary between two phases is an important aspect and exerts an influence on the dissolution speed of the intermetallic. Figure 5.3 gives a plot of the concentration profile of Si inside the precipitate and inside the aluminium matrix. Because the AlFeSi intermetallic has a stoichiometric composition, the concentration is constant inside the AlFeSi intermetallic. The concentration profile of silicon is chosen as an illustration because Fe has a low solubity in the Al-matrix.

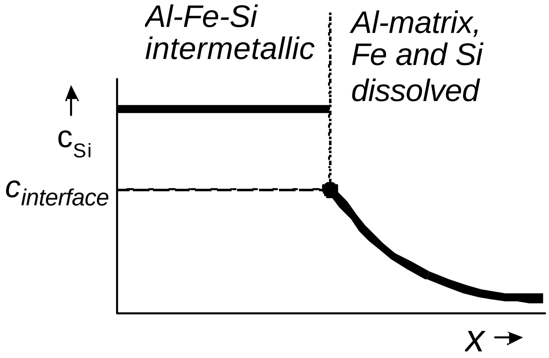

Figure 5.3 Schematic view of the concentration profile of Si. The matrix concentration on the boundary is indicated by the dot.

At the boundary of a *b*-AlFeSi phase there is an equilibrium of the *b*-phase with the Al matrix and its soluted Fe and Si according to the equilibrium reaction:

$$b\text{-Al}_5\text{FeSi} \Leftrightarrow 5\text{Al} + [\text{Fe}]_{\text{Al}} + [\text{Si}]_{\text{Al}}. \tag{5.7}$$

Therefore, the concentrations on the boundary of the individual elements are coupled to each other with a solubility product. For a multiphase intermetallic in equilibrium with another metal or intermetallic the general equation can be expressed by the solubility product [Kittel]:

$$\prod_j a_j^{v_j} = K(T), \tag{5.8}$$

where a_j are the activities of each element or crystal structure, j is the number of components that take part in the equilibrium process, and v_j are the prefactors of the equilibrium formula. $K(T)$ is the equilibrium constant, which has an Arrhenius type of relation:

$$K(T) = K_0 \exp\left(\frac{-Q}{RT}\right), \tag{5.9}$$

where K_0 is the prefactor and Q is the activation energy. In the case of equilibrium reaction 5.8: the components are Al_5FeSi, $[\text{Fe}]_{\text{Al}}$, $[\text{Si}]_{\text{Al}}$, and $[\text{Al}]_{\text{Al}}$. The activity of Al_5FeSi is equal to unity because it is a crystal. The activities of Fe and Si are equal to the concentrations inside the Al matrix: $a_2=\left[c_{Fe_{Al}}\right]_{interface}$ and $a_3=\left[c_{Si_{Al}}\right]_{interface}$. In the case that $a_{Al}=\left[c_{Al}\right]_{interface}$ one gets the solubility product of the β interface with its boundary:

$$\left[c_{Al}\right]^5{}_{interface} * \left[c_{[Fe]_{Al}}\right]_{interface} * \left[c_{[Si]_{Al}}\right]_{interface} = K(T). \tag{5.10}$$

Table 5.2 gives solubility products of different intermetallics found inside the Al matrix. Little literature is found on the solubility product of AlFeSi. Fe has a low solubility in aluminium (~0.05 wt%), and therefore it is possible that equation 5.10 does only hold for low Fe concentrations, or another solubility relation than 5.10 will hold. If Fe will not diffuse away, we are really talking about transformation, i.e. Si diffuses out which will give another Si/Fe ratio locally. This may give a new atomic arrangement and can result in a new phase.

TABLE 5.2, THE COEFFICIENTS OF THE SOLUBILITY PRODUCT OF DIFFERENT INTERMETALLICS INSIDE AN ALUMINIUM MATRIX [GRONG].

	Mg_2Si	CuMg	MgZn	Zn_2Mg
K_0 (wt%)$^{2 \text{ or } 3}$	$707.9 \cdot 10^3$	$4.36 \cdot 10^6$	$213.7 \cdot 10^3$	$52.48 \cdot 10^6$
Q_0 (Jmol^{-1})	$95.91 \cdot 10^3$	$76.67 \cdot 10^3$	$57.14 \cdot 10^3$	$81.46 \cdot 10^3$

5.1.3 The diffusion controlled velocity of an intermetallic interface

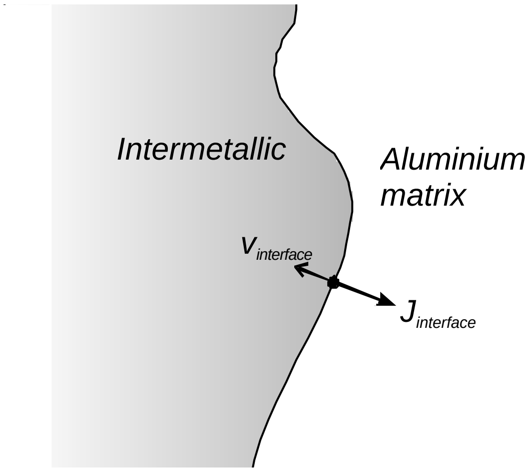

Figure 5.4 The velocity of the boundary is dependent of the diffusion flux on the boundary.

The velocity of the boundary of an intermetallic (see Figure 5.4) is diffusion controlled in the case that the time that a concentration equilibrium to be formed at the boundary is less than the diffusion rate away from the boundary into the matrix. Therefore, in the case of diffusion controlled growth or dissolution, the velocity of the boundary mainly depends on the diffusion rate, and a concentration equilibrium can be assumed at the boundary. The concentrations of Fe, Al and Si inside the precipitate ($c_{particle}$) are kept constant because the precipitate is stoichiometric. Now the interfacial velocity can be expressed by [Verm98]

$$v = \frac{J_{interface\ j}}{c_{partical\ j} - c_{int\ j}}, \qquad (5.11)$$

where *j* = Fe or Si and $J_{interface\ j}$ is the diffusional flux of element Fe or Si. $c_{int\ j}$ is the concentration of the Al-matrix on the interface. By deriving equation 5.11 it is assumed that the densities in the whole system (precipitate and matrix) are uniform: This assumption implies that there is no volume change of the total system due to dissolution of the particle inside the aluminum matrix. Further it is assumed that the concentration gradients parallel to the interface are negligible, and therefore all diffusional fluxes are perpendicular to the boundary.

5.1.4 Instabillities due to curvatures

As a morphological change occurs during homogenisation of AlFeSi intermetallics, it is interesting to look at possible mechanisms for this. A possible explanation is morphology instabilities due to curvature on the interface. The concentration on the boundary of one particle changes with the curvature. If the surface is rough, the rounded shapes will have different concentrations on the boundary than the flat interfaces and this will give concentration gradients parallel to the interface. Those gradients will give concentration fluxes parallel to the boundary, which will gives instabilities to the morphology of the intermetallics.

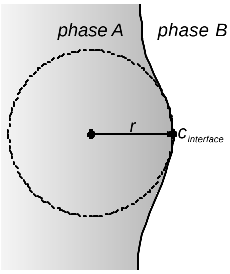

Figure 5.5. Local curvature r on the interface of phase A and B indicated by the dot. The interface concentration inside the Al-matrix depends on the local curvature of the interface.

In the cases of equation (5.10) no curvature is taken into account. But, if the interface is curved, as shown in Figure 5.5, the local concentration on the interface is also dependent on its local curvature. A curvature on the boundary raises or lowers the pressure inside the intermetallic. Usually this phenomenon is referred as the capillarity or the Gibbs-Thomson effect. The Gibbs-free energy change *DG* between a plate like and a curved particle is

$$\Delta G = g_{curved} - g_{plate} = \frac{2gV_m}{r}\ , \tag{5.12}$$

where V_m is the molar volume of the precipitate (m^3mol^{-1}), *r* is the radius of curvature at that point [m] as depicted in the figure, and *g* is the particle/matrix interfacial energy (J/m^2). This effect is schematically shown in Figure 5.6, for a Al_3Fe system where also the Gibbs free energy curve of the matrix is depicted.

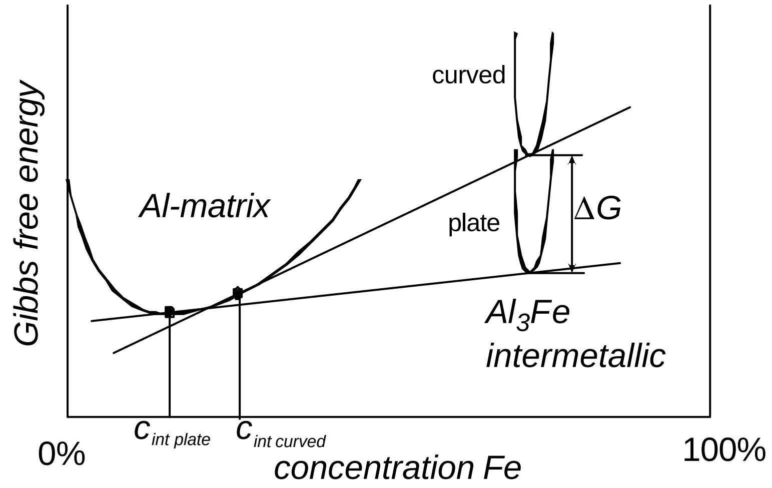

Figure 5.6 Gibbs free energy of a curved and plate morphology of the intermetallic.

Figure 5.6 shows that the particle curvature of an Al_3Fe intermetallic has an important effect on the concentration in the Al-matrix on the interfaces. Because the chemical potential of the intermetallics and the matrix have to be equal on the interface, tie lines are drawn which touch the free energy curves of the Al-matrix and the $AlFe_3$ intermetallic. Now it can be seen that the Fe concentration equilibrium with the aluminium matrix in the case of a particle with high interface curvature ($c_{int\ curved}$) is higher than the equilibrium concentration of a plate like particle ($c_{int\ plate}$). The concentration on the curved boundary can be expressed in terms of concentration on the boundary of a platelike sample by the relation [Gron97]:

$$c_{\mathrm{int}\ curved} = c_{\mathrm{int}\ \ plate} \cdot \exp\left(\frac{2gV_m}{RTr}\right). \tag{5.13}$$

It is possible to expand this equation for particles combining a number of chemical elements. Assuming that the same relationship also holds for intermetallics, a combination of equation (5.10) and (5.13) gives [Gron97]

$$\left[c_{Al}\right]^5{}_{interface} * \left[c_{[Fe]_{Al}}\right]_{interface} * \left[c_{[Si]_{Al}}\right]_{interface} = K(T) * \exp\left[\frac{2gV_m}{RTr}\right], \tag{5.14}$$

where *K(T)* is again an Arrhenius relation.

Sekerka and Martinis [Seke81] developed a model which deals with the morphological instability of a cylindrical particle during homogenisation (Figure 5.7a). As a result of local curvature differences, the concentration in the Al-matrix changes along the boundary (see equation 5.14). These concentration gradients will give diffusion fluxes along the boundary, as indicated by the small arrows in Figure 5.7a. Now an idea of the instability can be obtained from the Figure: the hills will grow and the valleys will get deeper. Using the perturbation theory, Sekerka and Martines calculated the fastest growing spatial wavelength along the interface. Without going in further details, it was demonstrated that this wavelength l is equal to:

$$l = 2.06 \cdot 2pr\ , \tag{5.15}$$

where r is the radius of the cylinder. After longer homogenisation times the cylinder will break up to spheres as shown in Figure 5.7b. Now, the wavelength of the perturbations given by equation 5.15 will be an estimation of the spatial wavelength of the formed spheres.

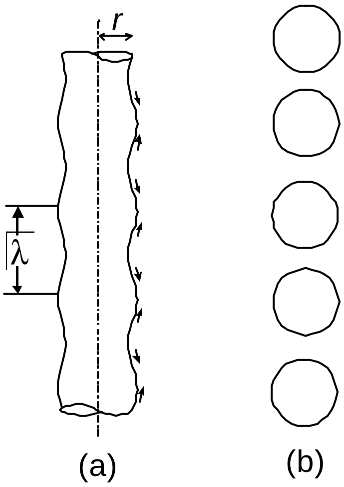

Figure 5.7 a) Morphology instability of a cylindrical precipitate during homogenisation. For clarity of presentation the radius is exaggerated. The diffusion fluxes along the boundary are indicated on the right side of the precipitate. b) After a longer homogenisation time the cylinder will break up in spheres.

5.2 Growth of new type of intermetallics and phase transformations

5.2.1 Introduction

The transformation of *b*- to *a*-intermetallics during homogenisation can be described by a general Avrami type of equation [Christ75], given by

$$X = 1 - \exp(-kt^n)\,, \tag{5.16}$$

where X is the fraction of intermetallics which are transformed, n is a time exponent and k is a kinetic constant which depends on the nucleation and growth rates. Considering the case that at t=0 only *b*-articles are present, the volume fraction X is defined as

$$X = \frac{V_a}{(V_b)_{t=0}}\,, \tag{5.17}$$

where V_a is the volume fraction of α particles and $(V_b)_{t=0}$ is the volume of β particles in a sample at the start of homogenisation. Few investigations have been performed on the transformation speed and kinetics for *b* - to *a* -transformation, so it can not be said that the Avrami equation holds for this type of transformation. However, the Avrami equation is found to be true for other peritectoid reactions e.g. Ree *et al.* [Ree91] for the peritectoid reaction $3U + U_3Si_2 \rightarrow 2U_3Si$ and Schulson *et al.* [Schul76] for Zr +Zr2Al → Zr_3Al.

The *b*- to *a*-AlFeSi transformation can be described by the peritectoid reaction:

$$b + \text{Al-matrix} \rightarrow a\,. \tag{5.18}$$

The process of growing is *diffusion controlled* if the diffusion speed is the limiting factor for growing. The next section will deal with diffusion controlled peritectoid reactions. On the other hand, if the reaction speed on the interfaces of the α-and β-intermetallic is slower than the diffusion speed, the rate of the transformation depends mainly on the reaction rate. Now the transformation is *reaction controlled.*

Christian [Christ75] found that the n in Avrami's equation 5.16 is dependent on the shape of the formed particle and the type of growth. The exponential growth law given by Avrami's equation is valid for linear growth (e.g. reaction controlled and nucleation controlled) under most circumstances, and approximately valid for the early stages of diffusion controlled growth. Table 5.3 gives some values of n which may be valid for β- to α-intermetallics transformation. It must be noted that the n's of Table 5.3 are obtained of the eutectoid type of transformations, and no n's of peritectoid reactions are obtained.

Table 5.3 Values of *n* in various growing conditions [Chist 75].

n	Condition
	Polymorphic changes, discontinuous precipitation, eutectoid reactions, interface controlled growth, etc:
4	Constant nucleation rate in time
3-4	Decreasing nucleation rate in time
	Diffusion controlled growth:
1 ½	All shapes growing from small dimensions, zero nucleation rate
1	Thickening of cylinders (needles)
½	Thickening of very large plates

5.2.2 Diffusion controlled growth of a peritectoid phase transformation

Fe has a very low solubility, and therefore almost no Fe will dissolve in or out the intermetallic during homogenisation. To form the equilibrium α-phase, Al and Si has to release from the intermetallics to dissolve in the Al-matrix, which was already shown in the peritectoid reaction (4.2):

$$2\beta\text{-Al}_5\text{FeSi} \rightarrow \alpha\text{-Al}_8\text{Fe}_2\text{Si} + 2\text{Al} + [\text{Si}]_{\text{Al}}, \qquad (5.19)$$

where $[\text{Si}]_{\text{Al}}$ is the silicon which diffuses out of the β-Al_5FeSi intermetallic and into the Al-matrix. It is possible that during the transformation a new α layer will form on a β particle as shown in Figure 5.8. The diffusion of Al and Si will go from the β-phase through the α-phase, and the α-layer will continue to grow until an complete α-particle is formed. However, in the intermediate time of transformation, cored particles are formed which are not reported in literature, so it is very doubtful if the transformation goes like this. But, it is plausible that the α phase starts to nucleate at one point of the boundary (instead of starting with a small core around the boundary), where after the nucleated α-phase begins to grow with a peritectoid diffusive controlled growth mechanism. This nucleation mechanism was also obtained by Zajec *et al.* [Zaja94] as was shown in the previous chapter, Figure 4.3.

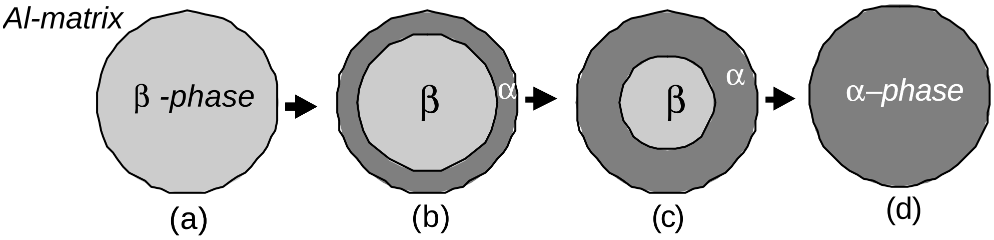

Figure 5.8 Peritectoid phase transformation of a spherical b-particle to a a-particle. In the intermediate phase transformations (b and c) cored particles are formed.

Fewer investigations and numerical calculations are performed on peritectoid reactions [Das99, Mehr96]. Picture 5.9 gives a general plate-like problem of multiphase diffusion.

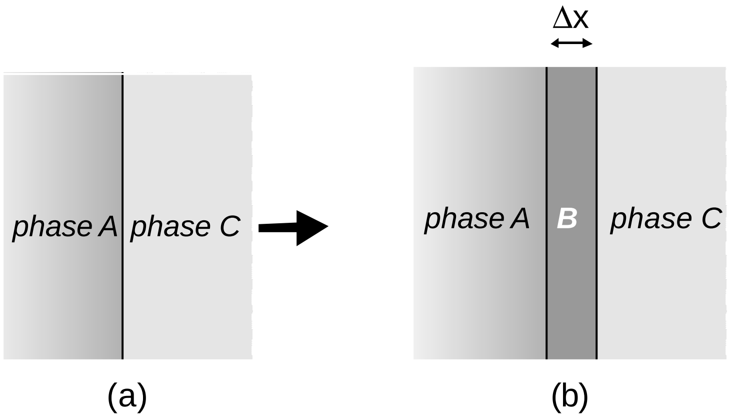

Figure 5.9 Diffusion couple of two phases A and C which forms by a peritectoid reaction to phase B

If there is local thermodynamic equilibrium at the boundary, the process is diffusion controlled. For this case, it is found that the thickness *Dx* of the growing intermetallic layer *B* (see Figure 5.9) in a binary system obeys a parabolic growth law [Mehr96], given by

$$\Delta x^2 = 2kt. \tag{5.20}$$

In most type of transformation the growth constant k increases with temperature according to an Arrhenius law

$$k = k_0 \cdot \exp\left(\frac{Q}{RT}\right). \tag{5.21}$$

Kidson [Mher96] has shown that the coefficients k_0 and Q are dependent of the equilibrium compositions on the interfaces and the interdiffusion coefficient in the Al-matrix and the intermetallics. (The interdiffusion coefficient is a diffusion coeficient of an element when more than one elements are dissolved in a phase [Port92]). However diffusion coefficents inside intermetallics are not in general well known.

6. Summary

For 6xxx Al alloy series the most frequently observed intermetallics are the monoclinic β-Al_5FeSi, cubic α_c-$Al_{12}Fe_3Si$ and hexagonal α'-Al_8Fe_2Si. Other less frequently observed intermetallics are the monoclinic β', rhombodhedral α_R, c-Centred orhorhombic α'', c-Centred monoclinic α_T, Monoclinic θ_2, and Monoclinic α_v.

During casting, intermetallics are formed between the arms of the solidifying aluminium dendrites. Fe has a very low solubility in the solid aluminium (~ 0.05 wt% at equilibrium), and therefore the Fe remains in the liquid aluminium until the last moments of solidification, and solidifies in the form of a β or an α_c second phase intermetallic. The morpology of cast β and α_c intermetallics (with the same dimensions) are very different. The β phase crystallizes as moderately curved planes, which are needle like in morpology, whilst α_c consists of strongly curved crystals which appear in the form of “Chinese script”.

The Fe/Si [wt%/wt%] alloy composition ratio and the solidification cooling rate during casting are two important parameters which determine whether β or α_c particles are formed. At industrial cooling rates of ~5 K/s or lower, a low Fe/Si ratio (<1) results in formation of β particles, while a high Fe/Si ratio (>1) results in α_c particles. Further, cooling rate of greater than ~5 K/s results in cubic α_c particles over wide range of Fe/Si ratios. β or α_c phases may form during casting by a number of different mechanisms:

- β or α_c intermetallics are formed directly from the liquid, which depends on the corresponding metastable liquid phase field of the alloy. This phase fields shifts as the cooling rate changes, and therefore the formation of β or α is also dependent of the cooling rate.
- Competitive growth and/or competitive nucleation suppress the β phase by the α phase at high cooling rates. Similar, the α phase is suppressed by the β phase at lower cooling rates.
- During casting, first α intermetallics are formed, which are transformed to β particles as a result of peritectic reactions.

During homogenisation the metastable platelike β intermetallics transform to the more favourable smaller and rounded α intermetallics. This transformation takes place only when the β-phase is present outside its own phase field equilibrium, and the corresponding phase field belongs to the α-phase.

The hexagonal α' phase is probably the equilibrium phase after long homogenisation times in 6xxx alloys with low Mn contents (0.001 wt%).When the manganese content is higher, however, the cubic α_c becomes the stable phase.

It is possible that the phase transformation form β to α_c proceeds by a peritectoid reaction in the following manner:

- α particles are nucleated on the boundary of β phases, and the β plates are gradually replaced by a uniform dispersion of α particles.
- The islands of α then thicken and sphereoidise at the expense of the remaining β-phase. During the peritectoid transformation silicon dissolves in the Al-matrix. The morphology change may be a result of instabilities caused by the Gibbs-Thomson effect.
- After the transformation, the thickness of the particles increase as a result of coarsening.

It is found that the rate of the transformation is effected by the grain size of the alloy. However, in this study the grain size was changes by addition of the grain refiner TiB_2, and the effect of those elements on the transformation kinetics was not discussed.

The b to a transformation is significantly accelerated by additions of small amounts of manganese (e.g. 0.05 wt%), and this is of great benefit to the extrusion industry. The reason for this acceleration may be that manganese gives a shift of the a-phase field. However, it can also be discussed that the acceleration is caused by forming cubic a_c-Al$_{12}$(Fe,Mn)$_3$Si phase, which exhibits a faster nucleation rate and faster growth speed than that of the hexagonal a¢-Al$_8$Fe$_2$Si, formed in pure Al-Fe-Si alloys.

The transformation of b to a type of intermetallics during homogenisation may be described by a general Avrami type of equation, which describes the volume fraction of transformed intermetallics as a function of the time. A parameter in this equation gives an indication whether the growth is diffusive controlled, nucleation controlled or reaction controlled.

Modelling of the b- to a-AlFeSi phase transformation looks promising, however, more experimental work needs to be performed to aford a better understanding of the main mechanisms of the phase transitions. Also the influence of Mn on the transformation rate appears very important, and may prove to be a useful tool in determining the nature of the b- to a- transformation.

References

[Alle98] C.M. Allen, K.A.Q. O'Reilly, B. Cantor, P.V. Evans, *Intermetallic phase selection in 1xxx Al alloys*, Progress in Materials Science, **43** (1998) pp. 89-170.

[Alex70] W.B. Alexander, L.M. Slifkin, Phys. Rev. B, **1** (1970) pp. 3274.

[Back68] L. Bäckerud, *Kinetic aspects of the solidification of binary and ternary alloy systems*, Jernkont. Ann., **152** (1968) pp. 109-138.

[Beke87] D.L. Beke, I. Gödény, I.A. Szabó, G. Erdélyi, F.J. Kedves, Philos. Mag., **A5** (1987) pp. 425.

[Berg73] D. Bergner, E. Cryrener, Neue Hütte, **18** (1973) pp. 356.

[Biro98] Y. Birol, *Formation and Transformation of Intermetallic Particles in Strip-cast Al-0.8Fe-0.6Si Alloy*, Z. Metallkd., **89** (1998) pp. 7.

[Coop66] M. Cooper, K. Robinson, Acta Cryst., **20** (1966) pp. 614.

[Coop76] M. Cooper, Acta Cryst., **23** (1967) pp. 1106.

[Clod86] M. P. Clode, T. Sheppard, *Surface generation and origin of defects during extrusion of Al alloys*, Proc. of Conf. Al. Techn. '86, Londen, (1986) pp. 230-239.

[Das99] A. Das, I. Manna, S.K. Pabi, *A Numerical Model of Peritectoid Transformation*, Metallurgical and Materials Transactions A., **30A** (1999) pp. 2563-2573.

[Donn94] P.Donnadieu, G. Lapasset, B. Thanaboonsombut, T.H. Sanders Jr, *a-phase particles in 6xxx aluminium alloys*, The 4th International Conference held in Atlanta, Georgia, USA 11-16 September, (1994) pp. 668-675.

[Dons84] A.L. Dons, *AlFeSi-particles in Commercial Pure Aluminium*, Z. Metallkde, **75** (1984) pp. 170-174.

[Dons85] A.L. Dons, *AlFeSi-Particles in Industrial Cast Aluminium Alloys*, Z. Metallkde, **76** (1985) pp. 609-612.

[Dons86] A.L. Dons, *AlFeSi-Particles in Commercial Pure Aluminium II*, Z. Metallkde, **77** (1986) pp. 126-130.

[Fuji77] S.-I. Fujikawa, *Diffusion of Magnesium in Al-Mg-Si Alloys*, Defect and Diffuison Forum, **143-147** (1997) pp. 403-308.

[Fuji78] Fujikawa S, Hirano K, Fukushima Y, *Diffusion of Silicon in Aluminum*, Metallurgical Transactions A, **9A** (1978) pp. 1811-1815.

[Grig89] A. Griger, V. Stefániay, A. Lendvai, T. Turmezey, *Possible modification of cast structure by continuous casting technology in AlFeSi alloys Part III: Intermetallic phases*, Aluminium 65, **10** (1989) pp. 1049-1056.

[Grig96] A. Griger, V. Stefániay, *Equilibrium and non-equilibrium intermetallic phases in Al-Fe and Al-Fe-Si Alloys*, Journal of materials science, **31** (1996) pp. 6645-6652.

[Gron97] O. Grong, *Metallurgical modelling of welding*. published by the Institute of Materials, 1 Carlton House Terrace, London, Sw1y5DB, 303, (1994).

[Hood70] G.M. Hood, Philos. Mag., **21** (1970) pp. 305.

[Lamb79] H.J. Lamb, *The Effect of trace additions of manganese and prior heat-treatment on the structure of dilute Al-Mg-Si Alloy extrusion ingot*, Proc. Conf. Institution of Metallurgist, **3V** (1979) pp. 4-5.

[Lang86] J. Langerweger, *Influence of heat treatment practice on extrudability and properties of AlMgSi alloy selections*, Proc. of Conf. Aluminium Techn. 1986, (1986) pp. 216-222.

[Lang90] Y. Langsrud, *Silicon in commercial aluminium alloys –what becomes of it during DC-casting?*, Key Engineering Materials, **44,45** (1990) pp. 95-116.

[Liu86] P. Liu, T. Thorvaldsson, G.L. Dunlop, *Formation of intermetallic compounds during solidification of dilute Al-Fe-Si alloys*, Materials Science and Technology, **2** (1986) pp. 1009-1018.

[Liu88] P. Liu, G.L. Dunlop, *Long-range ordering of vacancies in bcc α-AlFeSi*, Jourunal of materials science, **23** (1988) pp. 1419-1414.

[Mehr96] H. Mehrer, *Diffusion in Intermetallics*, Materials Transactions, JIM, **37**, No. 6 (1996), pp. 1259-1280.

[Mond76] L.F. Mondolfor, *Aluminium Alloys: Structure and Properties*, Published by Butter Worths & Co Ltd, London-Boston, (1976), pp. 534-567.

[Mula96] M.H. Mulazimoglu, A. Zaluska, J.E. Gruzleski, F. Paray, *Electron Microscope Study of Al-Fe-Si Intermetallics in 6201 Aluminum Alloy*, Metallurgical and Materials Transactions A, **27A** (1996) pp. 929-936.

[Onur94] S. Onurlu, A. Tekin, *Effect of heat treatment on the insoluble intermetallic phases present in an AA6063 alloy*, Journal of Materials Science, **29** (1994) pp. 1652-1655.

[Port91] D.A. Porter, K.E. Easterling, *Phase transformations in metals and alloys*, Published by Chapman & Hall, 2-6 Boundary Row, London SE1 8HN, (1992).

[Rhee91] C. Rhee, S. Pyun, I. Kuk, *The kinetics of the peritecoid reaction* $3U + U_3Si_3 \rightarrow 2U_3Si$ *as a function of size of parent* U_3Si_2 *precipitate in the uranium matrix,* Journal of Nuclear Materials, **184** (1991) pp. 146-149.

[Roth74] S.J. Rothman, N.L. Peterson, L.J. Nowicki, L.C. Robinson, Phys. Status Solidi (b) **63** (1974) pp. 29.

[Schul76] E.M. Schulson and D.B. Graham, Acta Metall., **24** (1976) pp. 615.

[Seke81] R.F. Sekerka and T.F. Marinis, *Dynamics of morphological change during solid-solid transformations*, Proceedings Of An international Conference on Solid → Solid phase transformations, (1982) pp. 67-84.

[Skjer87] P. Skjerpe, *Intermetallic phases formed during DC-Casting of an Al-0.25 wt Pct Fe-0.13 Wt Pct Si Alloy*, Metallurgical Transactions A, **18A**, (1987) pp. 189-200.

[Stef87] V. Stefániay, A. Griger, T. Turmezey, *Intermetallic phases in the aluminium-corner of the AlFeSi-alloy system*, Journal of Materials science, **22** (1987) pp. 539-546.

[Tani96] H. Tanihata, K. Matsuda and S. Ikeno, *High Resolution Transmission Electron Microscope Observation of the Metastable Phase in an Aged Commercial AA6063*, Materials Science Formum, **217-222** (1996) pp. 809-814.

[Tani99] H. Tanihata, T. Sugawara, K. Matsuda, S. Ikeno, *Effect of casting and homogenizing treatment conditions on the formation of Al-Fe-Si intermetallic compounds in 6063 Al-Mg-Si alloys*, Journal of Materials Sciences, **34** (1999) pp. 1205- 1210.

[Turm87] T. Turmezey, *AlFe and AlFeSi intermetallic phases in aluminium alloys*, Materials Science Formum, **13/14** (1987) pp. 121-132.

[Verm98] F. J. Vermolen, *Mathematical Models for Particle Dissolution in Extrudable Aluminium Alloys*, Ph.D. Thesis, University of Technology Delft, (1998).

[West82] H. Westengen, *Formation of Intermetallic Compounds During DC Casting of a Commercial Purity Al-Fe-Si Alloy*, Z. Metaallkd, **73** (1982) pp. 360-368.

[Til00] W. van Til, C. Vuik, S. van der Zwaag, *An Inventory of Numerical Methods to model Solid-Solid Phase Transformations in Aluminium Alloys*, Internal report of the NIMR, (2000).

[Zaja94] S. Zajac, B.Hutchinson, A. Johansson, and L.-O. Gullman, *Microstructure control and extrudability of Al-Mg-Si alloys microalloyed with manganese*, Materials Science and Technology, **10** (1994) pp. 323.

[Zaja96] S. Zajac, L Gullman, A. Johansson, B Bengtsson, *Hot ductility of some Al-Mg-Si alloys*, Materials Science Forum, **217-222** (1996) pp. 1193-1198.